Atmos. Meas. Tech., 6, 275–299, 2013
www.atmos-meas-tech.net/6/275/2013/
doi:10.5194/amt-6-275-2013

Atmospheric Measurement Techniques
Open Access

Retrieval interval mapping: a tool to visualize the impact of the spectral retrieval range on differential optical absorption spectroscopy evaluations

L. Vogel[1], **H. Sihler**[1,2], **J. Lampel**[1], **T. Wagner**[2], **and U. Platt**[1]

[1]Institute of Environmental Physics, University of Heidelberg, Im Neuenheimer Feld 229, 69120 Heidelberg, Germany
[2]Max Planck Institute for Chemistry, Hahn-Mertner-Weg 1, 55128 Mainz, Germany

Correspondence to: L. Vogel (leif.vogel@iup.uni-heidelberg.de), H. Sihler (holger.sihler@iup.uni-heidelberg.de)

Received: 15 March 2012 – Published in Atmos. Meas. Tech. Discuss.: 13 June 2012
Revised: 24 December 2012 – Accepted: 3 January 2013 – Published: 7 February 2013

Abstract. Remote sensing via differential optical absorption spectroscopy (DOAS) has become a standard technique to identify and quantify trace gases in the atmosphere. Due to the wide range of measurement conditions, atmospheric compositions and instruments used, a specific challenge of a DOAS retrieval is to optimize the retrieval parameters for each specific case and particular trace gas of interest. Of these parameters, the retrieval wavelength range is one of the most important ones. Although for many trace gases the overall dependence of common DOAS retrieval on the evaluation wavelength interval is known, a systematic approach for finding the optimal retrieval wavelength range and quantitative assessment is missing. Here we present a novel tool to visualize the effect of different evaluation wavelength ranges. It is based on mapping retrieved column densities in the retrieval wavelength space and thus visualizing the consequences of different choices of spectral retrieval ranges caused by slightly erroneous absorption cross sections, cross correlations and instrumental features. Based on the information gathered, an optimal retrieval wavelength range may be determined systematically.

The technique is demonstrated using examples of a theoretical study of BrO retrievals for stratospheric BrO and BrO measurements in volcanic plumes. However, due to the general nature of the tool, it is applicable to any type of DOAS retrieval (active or passive).

1 Introduction

Differential optical absorption spectroscopy (DOAS) is an established technique to quantify the concentration and distribution of a large number of atmospheric gases in the ultraviolet (UV), visible (Vis) and near-infrared (NIR) wavelength ranges (Platt and Stutz, 2008). The technique is based on the Lambert–Beer law (also known as Bouguer–Lambert law), which states that the intensity of electromagnetic radiation with an initial intensity I_0 will decrease exponentially depending on the amount of absorber present and its respective absorption cross section. The idea behind DOAS is to split the absorption cross section $\sigma(\lambda)$ in its broad-band and narrow-band parts (absorption structures widths typically smaller than a few nm). This narrow-band part is also called the differential absorption. Thus it is possible to determine the amount of various gases with sufficiently strong differential absorption features by splitting the total absorption into broad-band extinction and narrow-band absorption. A suitable filter such as a polynomial can be applied to describe the combined broad absorption structures together with Rayleigh and Mie extinction and broad-band instrumental features, whereas the amounts of trace gases of interest are derived from their narrow-band absorption structures. Due to the differences in differential absorption structures, it is possible to retrieve different trace gases in the same measurement and spectral region. In this case, the recorded intensities need to be carefully separated in order to determine the integrated concentration of the trace gases along the light path, the slant column density (SCD). In many scenarios, the absorption of the trace gas of interest is concealed

Table 1. Selection of published DOAS measurements of BrO and the respective retrieval wavelength intervals used for the DOAS evaluation. The list is ordered by ascending lower wavelength limit and type of measurement (ground-based and airborne in the upper part, satellite instruments in the bottom part). The index number is given for orientation and further reference in later figures. In general, the list indicates the broad range of wavelength intervals applied.

Index	Lower Limit [nm]	Upper Limit [nm]	Type of measurement	Reference
1	310.9	377.8	MAX-DOAS, volc. plume	Boichu et al. (2011)
2	320	360	MAX-DOAS, volc. plume	Bobrowski and Platt (2007)
3	324	354	Airborne, volc. plume	Heue et al. (2011)
4	330	373.6	Airborne, volc. plume	Bani et al. (2009)
5	332	352	MAX-DOAS, volc. plume	Bobrowski and Platt (2007)
6	335.3	358.9	MAX-DOAS, Arctic	Wagner et al. (2007)
7	340*	359*	MAX-DOAS, m.b.l.	Coburn et al. (2011)
8	344.7	359	Zenith sky	Richter et al. (1999)
9	346	358	Zenith sky	Otten et al. (1998)
10	346	359	Zenith sky	Aliwell et al. (2002)
10	346	359	MAX-DOAS, Arctic	Hönninger et al. (2004)
10	346	359	Airborne, Arctic	Prados-Roman et al. (2011)
10	346	359	MAX-DOAS, volc. plume	Bobrowski and Platt (2007)
11	346.5	359.2	MAX-DOAS, m.b.l.	Leser et al. (2003)
12	319	347.5	OMI	Salawitch et al. (2010)
13	336	347	SCIAMACHY	Afe et al. (2004)
13	336	347	GOME-2	Begoin et al. (2010)
14	336	351.1	GOME-2	Valks et al. (2009)
15	336	351.5	SCIAMACHY	De Smedt et al. (2004)
16	336	352	GOME-2	Theys et al. (2009)
17	336	360	GOME-2	Heue et al. (2011)
17	336	360	GOME-2	Sihler et al. (2012)
18	344.5	359	OMI	Chance (1998)
19	344.7	359	GOME	Richter et al. (1998)
20	345	359	GOME	Richter et al. (2002)
20	345	359	OMI	Chance (2002)
21	345	359.5	GOME	Wagner and Platt (1998)
22	346	359	GOME	Hegels et al. (1998)
22	308	341	LP-DOAS, Arctic	Poehler et al. (2010)
23	310	340	LP-DOAS, Arctic	Tuckermann et al. (1997)
24	312	357	LP-DOAS, Arctic	Hönninger et al. (2004)
25	315.5	348	LP-DOAS, Arctic	Liao et al. (2011)
26	317	358	LP-DOAS, m.b.l.	Saiz-Lopez et al. (2004)
27	324	357	LP-DOAS, m.b.l.	Mahajan et al. (2010)
28	327	347	LP-DOAS, salt lake	Matveev et al. (2001)
29	329**	347**	LP-DOAS, salt lake	Hebestreit et al. (1999)
30	331	357	LP-DOAS, volc. Plume	Kern et al. (2009)
31	332***	351***	LP-DOAS, Arctic	Stutz et al. (2011)

* In addition, Coburn et al. (2011) applied a significance criterion consisting of logical AND combination of a 2-band (345–359 nm) and a 3-band (340–359 nm) evaluation of BrO (personal communication, October 2012). ** derived from Hebestreit et al. (1999), Fig. 1. *** 338.7–342.3 nm and 346.1–347.4 nm excluded..

by the presence of stronger absorbers. Small errors in reference absorption cross sections (RCSs) might lead to small errors in the determination of the strong absorber, but can heavily influence the retrieval results of other much weaker absorbers.

DOAS instruments can be classified into active and passive instruments, which apply artificial light sources or natural light sources (scattered sun, direct sun, moon or starlight), respectively. Active DOAS instruments allow one to compare spectra of light before and after a beam has passed a known distance through a volume of air containing the absorbing gas. For practical purposes, long-path instruments (LP-DOAS) are limited by the necessity of the stable deployment of a light source, receiver as well as additional reflectors (e.g. Merten et al., 2011, and references therein). This may not be necessary for cavity-enhanced DOAS (CE-DOAS) (e.g. Platt et al., 2009). Passive instruments can be constructed to be very compact and of low power consumption since they do not require an additional emitter and reflectors. Applications include satellite measurements or Multi-AXis DOAS

(MAX-DOAS) from different platforms (ground-based, aircraft, balloon, ships and car traverses), which have been applied to a multitude of scientific problems including measurements of volcanic plumes. For a comprehensive overview of different DOAS systems and the evaluation technique, see Platt and Stutz (2008).

The wavelength interval in which the DOAS retrieval is performed is one of the most important parameters of the retrieval process. Obviously, the interval should include prominent absorption features of the trace gas of interest in order to obtain optimum sensitivity, whilst excluding strong absorptions features of other trace gases and possible instrumental artefacts. Thus, a balance has to be found between sensitivity and possible cross correlations. A broader interval increases the information available to the algorithm, but also introduces the danger of incorporating the strong absorption structures of other gases present. In some cases, a broader wavelength range can increase errors due to insufficient correction of the broad-band terms (Marquard et al., 2000; Puķite et al., 2010). Other effects to be considered are the wavelength dependency of the Ring effect in presence of higher aerosol loads or clouds (e.g. Wagner et al., 2009, and references therein) and radiative transfer effects when measuring volcanic plumes (Kern et al., 2010). A narrower evaluation wavelength range on the other hand can lead to an increase in cross correlation between the different RCSs. Moreover, the retrieval might be more strongly influenced by the DOAS high-pass filtering (e.g. fitting of a polynomial).

Despite the importance of the problem, only a few attempts were made to systematically and quantitatively assess the influence of the retrieval wavelength range on the resulting SCDs. In most publications, the retrieval wavelength ranges applied are only motivated by a single comparison to one other retrieval wavelength range. Furthermore, a large variety of retrieval wavelength intervals have been used by different authors. This is illustrated in Table 1, which displays a selection of different retrieval wavelength ranges of bromine monoxide (BrO), which have been used in the past. Since the studies of BrO in Table 1 have been performed with different instruments from different platforms and strongly varying measurement conditions, a single retrieval wavelength interval would not have been sufficient. Nevertheless, one wonders whether a total of 32 different retrieval wavelength intervals really represents the different requirements of the various measurement geometries and instruments used.

One of the few systematic studies on the retrieval of BrO was published by Aliwell et al. (2002), where DOAS retrievals were studied for measurements of stratospheric BrO via ground-based zenith-looking instruments at mid-latitudes. In that case, one faces lowBrO SCDs combined with very high ozone O_3 SCDs, which interfere with the evaluation since measurements are conducted at a high solar zenith angles (SZA). Aliwell et al. (2002) found an optimal retrieval range from 346 nm to 359 nm, which limits cross correlations with O_3 but encompasses only two, relatively weak, BrO absorption bands in the retrieval. Theys et al. (2007) supported the suggested wavelength range with an additional radiative transfer study. The results of these studies, however, can not be unambiguously transferred to the retrieval of BrO under any measurement condition (differences in BrO SCDs, SZA, time difference between the measurement of the Fraunhofer reference spectrum and the measurement spectrum, etc.). Similar studies for other measurement conditions and trace gases are sparse (for NO_2, e.g. Roscoe et al., 2010). Furthermore, the effects of different retrieval intervals have not been studied systematically over a broad range of retrieval intervals for any trace gas.

In this study, we introduce a novel tool that is suitable for systematically and quantitatively studying the influence of the retrieval wavelength interval on the results and quality of the DOAS retrieval. It consists of contour plots of DOAS retrieval results where the lower and upper limits of retrieval wavelength intervals are the coordinates, while the value of retrieved column density or the value of any other retrieval parameter of interest (e.g. fit error, χ^2 value as a measure of the overall goodness of the fitting algorithm's results, possible shifts in wavelength calibration by the algorithm) is plotted colour coded (see Sect. 2). These retrieval maps enable an easy visualization of the results for a large set of evaluation wavelength ranges and offer an intuitive tool for showing how certain key parameters influence the fit results.

One problem when analysing the influence of the retrieval wavelength range is that the true SCDs of trace gases are usually unknown for measured spectra. Therefore, as an application example, synthetic spectra are studied with known columns of trace gases. These synthetic spectra represent simplified spectra of passive DOAS measurements of stratospheric BrO and BrO in volcanic plumes using scattered sunlight (see Sect. 3). Different tests are performed on these synthetic spectra as described in Sect. 3.3: (i) the influence of the I_0 effect, (ii) cross correlations between trace gas RCSs and variations in assumed trace gas SCDs, and (iii) the behaviour of retrieved results when noise is added to the synthetic spectra. The results for each measurement set-up and test are presented and discussed in Sect. 4, followed by a general comparison between measurement scenarios in Sect. 5 and concluding remarks in Sect. 6.

2 Retrieval wavelength mapping – general approach

Small errors in reference cross sections (RCSs) and corrections for broad-band extinction, unaccounted radiative transfer effects, cross correlations between RCSs and instrumental defects may lead to erroneously retrieved slant column densities (SCDs) of measured trace gases. In general, these systematic errors exhibit a dependency on the retrieval wavelength interval, which varies more slowly over broader wavelength intervals than errors introduced by common pixel to

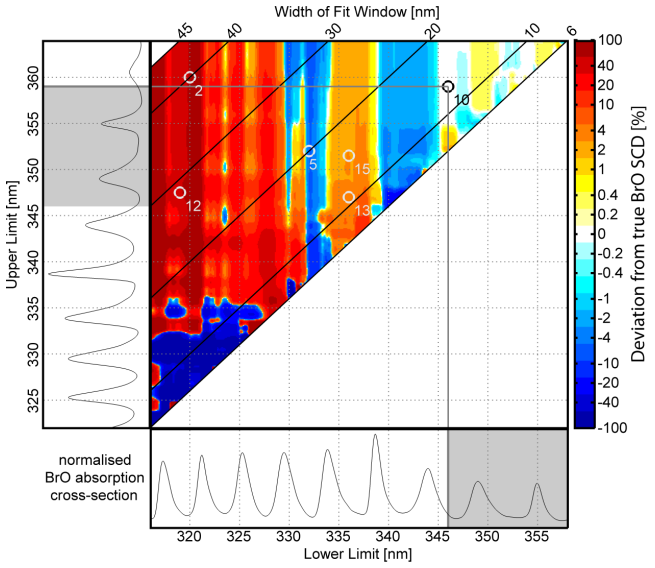

Fig. 1. Wavelength interval mapping of a synthetic spectrum. Zenith-sky measurements of stratospheric BrO (Table 2) are simulated with a true BrO SCD of 1.5×10^{14} molec cm^{-2}. The retrieval applies I_0-corrected RCSs. The abscissa axis shows the lower wavelength limit of the retrieval wavelength interval, the ordinate axis the upper wavelength limit. Deviations from the true BrO SCD are displayed on a logarithmic colour coded scale. The circles mark selected retrieval wavelength intervals in the literature, which are referenced by the given number in Table 1. The highlighted wavelength interval denotes the optimal retrieval wavelength interval found by Aliwell et al. (2002).

pixel sensitivity differences and electronic or photonic noise. Therefore, these different types of error should be distinguishable in a systematic study of the influence of retrieval wavelength intervals on the retrieved values.

A DOAS retrieval performed systematically over a wide range of different wavelength ranges may uncover these systematic variations and allows one to study key parameters. This includes among others the retrieval wavelength interval dependency of the following:

- retrieved trace gas SCDs and their fit error;
- cross correlations between different RCSs;
- the influence of parameters like wavelength calibration of spectra;
- radiative transfer effects;
- the influence of instrumental features;
- shifts in wavelength calibration of recorded spectra;
- the dependency of the retrieved SCDs on the I_0 effect and Ring effect (passive DOAS measurements only).

By studying appropriate parameters, an optimal retrieval wavelength range may be found which results in a robust retrieval of true trace gas slant columns. In this way, an optimal homogenization of retrievals may be achieved, which is necessary, e.g. if larger data sets are recorded by different instruments.

Easy visualization of such systematic retrievals can be achieved by displaying the results in contour plots, where the first and second dimension are the lower and upper limits of the retrieval wavelength interval respectively. The plotted results are colour coded. Thus each point in the plot corresponds to one particular wavelength interval. The resulting maps allows one to readily identify retrieval wavelength intervals which are likely to lead to erroneous results, or might lead to a greater variability of the retrieved SCDs due to a large gradient of the retrieval interval dependency.

As an example of this novel method, Fig. 1 displays retrieved BrO SCDs using a synthetic spectrum modelling zenith-sky DOAS measurements of stratospheric BrO. Details on the construction of the synthetic spectrum are given in Sect. 3. Since it is a synthetic spectrum, the true BrO SCD of 1.5×10^{14} molec cm^{-2} is known. All retrieval wavelength intervals are plotted with lower limits of 316–358 nm and upper limits of 322–364 nm. The respective wavelength limits are varied in steps of 0.1 nm, with a total width of the interval ω between 6 nm and 45 nm. Retrieval results which differ by less than 0.1 % from the true SCD are plotted in white; under- and overestimated results in shades of blue and red respectively. The advantage of this systematic approach is apparent. In a first assessment, certain retrieval wavelength intervals can be disregarded since they yield results that deviate quite strongly from the true value, while others could be subject to further investigation. For instance, evaluation intervals including wavelengths below $\approx$ 345 nm yield erroneous results. For an in-depth discussion of the depicted result, see Sect. 4.1.

The computational requirements to map the wavelength evaluation ranges are moderate. All individual maps shown were generated on a desktop PC with a 3.0 GHz processing unit. The retrievals necessary for a single map were performed with the software package DOASIS (Doasis, 2010; Kraus, 2006; Lehmann, 2013) within 30 min for the given wavelength evaluation ranges at 0.1 nm steps. Therefore, this novel tool allows one to give a quick overview of possible pitfalls in DOAS evaluations. An example is provided in the Supplement, which consists of the necessary DOASIS script to perform the evaluations and Matlab/Octave scripts to visualize the results as well as spectra and fit scenarios described in Sects. 3.1 and 3.2 to perform Test I (Sect. 3.3.1).

3 Retrieval wavelength mapping for the example of synthetic spectra

In order to give an example application of the method described above, synthetic spectra were generated simulating two different measurement scenarios: stratospheric BrO by

zenith-sky DOAS and BrO in tropospheric volcanic plumes. As mentioned above, synthetic spectra offer the advantage that retrieved and true SCDs can be compared. Both measurement scenarios assume passive DOAS measurements using scattered sunlight, allowing one to study the two different measurement conditions in direct comparison. In order not to exceed the scope of these examples, certain effects are neglected. The most important of these is the Ring effect (Grainger and Ring, 1962), which, if insufficiently corrected, may greatly affect the retrieval results due to its narrow-band structure. For a correct assessment of the Ring effect however, an extensive study including advanced radiative transfer modelling and comparison with measured data would be necessary. Up to date, the tools are missing to calculate the Ring effect in a 3-dimensional atmosphere in order to perfectly simulate the effect when probing volcanic plumes. Furthermore, retrieval wavelength ranges yielding highly erroneous SCDs without considering the Ring effect will not yield true SCDs when the effect is included. However, an attempt to assess the influence of the Ring effect is described in Appendix B, in which results need to be treated with care due to the above described difficulties. The effects of noise are neglected for certain tests (I and II, see Sect. 3.3) performed on the two measurement scenarios. Given these simplifications, the results can be assumed to yield the lowest error possible and act as a "best-case" scenario. This poses certain limits on extending the results from the studied synthetic measurement scenarios to spectra measured in the field. The prime focus of this study is to present the new method of retrieval wavelength mapping rather than model real measurement spectra.

The software package DOASIS was used for computation of all spectra and retrieval of results (Doasis, 2010; Kraus, 2006; Lehmann, 2013).

3.1 Generation of synthetic spectra

The same approach was taken for all measurement scenarios in constructing synthetic spectra as well as RCSs. Because this study focuses on measurements using scattered sunlight, a high-resolution solar spectrum $I_{\mathrm{K},0}$ (Kurucz, 2005) is used as an initial spectrum without additional absorption structures with a dispersion of $\approx 150/\left(3\times10^5\right)$ nm/pixels between 300 and 450 nm. The literature absorption cross sections of the different trace gases ($\sigma_i(\lambda)$, see Table 2) were recorded at different spectral resolutions. Thus they were first interpolated to $\sigma_{\mathrm{K},i}(\lambda)$ at the resolution of the initial solar spectrum $I_{\mathrm{K},0}$. Subsequently, the RCSs $\sigma_{\mathrm{K},i}(\lambda)$ were multiplied by the respective SCDs S_i assumed for each trace gas and measurement scenario. Their absorptions were applied to the solar spectrum $I_{\mathrm{K},0}$ according to the Lambert–Beer law:

$$I_{\mathrm{K}}(\lambda) = I_{\mathrm{K},0}(\lambda)\exp\left(-\sum_i \sigma_{\mathrm{K},i}(\lambda)\cdot S_i\right). \quad (1)$$

The high-resolution spectra with (I_{K}) and without absorptions ($I_{\mathrm{K},0}$) were convolved with an instrumental slit function W of Gaussian shape with 0.65 nm FWHM (full width at half maximum). A spectrometer with a detector of 1024 pixels was assumed with a spectral range of 300 nm–402.3 nm with a constant dispersion of 0.1 nm/pixel. This allows one to disregard possible under-sampling effects (Roscoe et al., 1996; Platt et al., 1997; Chance et al., 2005), and the results can be transferred to spectrographs of similar optical resolution and equal or higher dispersion. The calculated synthetic spectra are denoted I_0 and I_{M} for Fraunhofer reference and measurement, respectively. The I_0 spectrum constructed in this way was used as a Fraunhofer reference spectrum in all evaluations.

When convolving the high-resolution RCSs $\sigma_{K,i}(\lambda)$ to the resolution of the instrument, care must be taken to account for the I_0 effect (Platt et al., 1997), because the incident solar spectrum and the RCSs are highly structured. The convolution also introduces an error for absorbers at high optical densities ($\ln(I_0/I) > 0.1$). The reason for both effects is that the convolution and Lambert–Beer law do not commute (e.g. Wenig et al., 2005). In this study, RCSs are denoted as "uncorrected RCSs" if they are not corrected for the I_0 effect or saturation effect. They are constructed by convolving the RCSs $\sigma_{\mathrm{K},i}(\lambda)$ with the instrumental slit function W to the instrumental resolution.

RCSs corrected for the I_0 effect and saturation are calculated corresponding to (Platt et al., 1997; Aliwell et al., 2002; Wagner et al., 2002)

$$\sigma_i'(\lambda) = -\frac{1}{S_i}\ln\left(\frac{\left(\left[I_{\mathrm{K},0}\exp\left(-\sigma_i S_i\right)\right] * W\right)(\lambda)}{\left(I_{\mathrm{K},0} * W\right)(\lambda)}\right) \quad (2)$$

where $*$ denotes the convolution operation. However, using only the incident solar light $I_{\mathrm{K},0}$ in the denominator of Eq. (2) neglects the fact that many absorbers can be present at partly very high optical densities (e.g. O_3 in measurement scenario for zenith-sky DOAS, Sect. 3.2.1). Thus a true correction of the I_0 effect can only be achieved if a spectrum $I_{\mathrm{K}',0}$ is used in Eq. (2), which consists of $I_{\mathrm{K},0}$ modified by all other absorptions present except the one to be corrected. Although this can easily be achieved for synthetic spectra with known SCDs of absorbers, it would require a high computational effort if applied to measured spectra, which is not feasible for common DOAS retrievals.

3.2 Measurement scenarios

3.2.1 Measurements of stratospheric BrO by zenith-sky DOAS

In this scenario, spectra of ground-based zenith-sky DOAS measurements are simulated, which are used to measure stratospheric BrO. Commonly, spectra are recorded with a zenith looking telescope at high solar zenith angles (SZA). Evaluation of spectra at higher SZA against reference spectra at 70° SZA yields information about stratospheric trace gases. The main problem for retrievals of stratospheric BrO

Table 2. SCDs used in the construction of synthetic spectra for the two different measurement scenarios. The zenith-sky DOAS scenario corresponds to the composition of slant column densities typical for zenith-sky DOAS measurements of stratospheric BrO at mid-latitudes. It reproduces the settings in Aliwell et al. (2002). The second scenario, volcanic plumes, applies typical SCDs of trace gases for MAX-DOAS measurements of BrO in tropospheric volcanic plumes.

trace gas	temperature [K]	reference cross-section	zenith-sky DOAS [molec cm^{-2}]	volcanic plumes [molec cm^{-2}]
BrO	298 K	Fleischmann et al. (2004)	1.5×10^{14}	1.5×10^{14}
O_3	221 K	Burrows et al. (1999)	8×10^{19}	0
O_3	241 K	Burrows et al. (1999)	2×10^{19}	0
O_3	273 K	Burrows et al. (1999)	0	1×10^{18}
NO_2	220 K	Vandaele et al. (1998)	5×10^{16}	0
NO_2	294 K	Vandaele et al. (1998)	0	5×10^{16}
SO_2	298 K	Hermans et al. (2009); Vandaele et al. (2009)	0	1×10^{18}
CH_2O	298 K	Meller and Moortgat (2000)	0	3×10^{16}

measurements is the strong O_3 absorption structures encountered at lower wavelengths. The results can be transferred to other measurement scenarios under similar conditions (e.g. stratospheric balloon measurements, satellite measurements in the limb-viewing direction). Information on the assumed RCSs and SCDs is given in Table 2. The assumed columns for the zenith-sky DOAS scenario are the same as the ones used in a previous study by Aliwell et al. (2002). However, instead of the BrO cross section by Wahner et al. (1988) at 223 K, the cross section by Fleischmann et al. (2004) at 298 K was used, because the latter is available at higher resolution and the same BrO cross sections for both measurement scenarios can be used. Sensitivity tests have been performed for cross sections at different temperatures and by different authors (Wahner et al., 1988; Wilmouth et al., 1999; Fleischmann et al., 2004). Although the amplitude can differ significantly, the shape remains similar (see also Dorf, 2005). Since the BrO's optical density is small compared to the other absorbers, it can be assumed that the relative changes in retrieved SCDs are independent of the respective BrO RCSs used for all tests performed. This approach is also justified by the negligible differences in retrieved SCDs that can be seen in the results presented later between this study and Aliwell et al. (2002), Sect. 4.1.1.

3.2.2 BrO in tropospheric volcanic plumes

This scenario is set up to model tropospheric measurements of a volcanic plume at low-elevation viewing angles. The Fraunhofer reference spectrum would be recorded in zenith view, and it is assumed to be taken in close proximity in time with measurements of the volcanic plume and thus at approximately the same SZA. Consequently, the measurement will be sensitive to trace gases in the volcanic plume as well as to absorbers in the the lower ambient atmosphere. Stratospheric absorptions should be the same in both measurement and reference spectrum and cancel in the retrieval. Thus they are neglected in this scenario. Tropospheric SCDs of NO_2, O_3 and HCHO correspond to a slightly polluted troposphere, as found at Mt. Etna, Italy, during the summer months (Huijnen et al., 2010; Curci et al., 2010; Heckel et al., 2005). BrO and SO_2 SCDs are typical for a diluted plume, which is several minutes old at the point of the measurement (Bobrowski and Platt, 2007; von Glasow, 2010). Advanced modelled measurement scenarios are described in Vogel (2011).

These measurement conditions are quite different to those of zenith-sky DOAS. Since stratospheric O_3 absorptions are neglected, assumed SCDs of tropospheric O_3 are much smaller. However, the volcanic plume includes SO_2 at high concentrations, which absorbs in a similar wavelength range as O_3. Possible cross correlation of BrO with ambient HCHO must also be taken into account due to the similar shape of absorption structures and optical density encountered.

3.3 Tests performed on synthetic spectra

Several tests were performed on the two measurement scenarios. In order to allow for a better comparison between the different tests, only two different retrievals are used. A set of (1) uncorrected RCSs and (2) I_0-corrected RCSs for each scenario is applied. The different tests vary by small changes to the synthetic measurement spectra (variations of the SCDs of absorbers, added noise, etc.). Otherwise, all retrievals are performed coherently. In both evaluation scenarios, the logarithm of the Fraunhofer reference spectrum I_0 was fit together with the RCSs to the logarithm of the synthetic measurement spectrum I_M, instead of fitting the RCSs to the logarithm of the ratio I_M/I_0. This is a common approach in order to account for small shifts in wavelength-pixel mapping between the Fraunhofer reference and measurement spectrum, which can occur by temperature drifts of the optical bench of the spectrograph. The fit coefficient of the Fraunhofer reference was fixed to unity. The stability of the retrieval was ensured by only allowing the set of RCSs and Fraunhofer reference spectrum to shift and squeeze in wavelength as a whole. Furthermore, a DOAS polynomial

of second order was included. This is sufficient since no additional broad-band extinctions are applied during the construction of synthetic spectra. If the presented tool is applied to field measurements however, the effect on the retrieval results by different degrees of DOAS polynomials should be studied.

3.3.1 Test I: influence of the I_0 effect

As a first test, the influence of the I_0 effect on retrieved column densities was assessed by fitting both sets of RCSs (uncorrected and corrected for the I_0 effect) to the synthetic measurement spectrum. In this way, the upper limit of accuracy is established with which the different SCDs of respective measurement scenarios can be reproduced. This test also allows direct comparison to the study of Aliwell et al. (2002) for the zenith-sky DOAS measurement set-up.

As mentioned in Sect. 3.1, a true I_0 correction can only be achieved if the denominator $I_{K,0}$ in Eq. (2) includes absorptions of all trace gases except the one whose cross section is to be corrected. This was tested for both synthetic measurement spectra, and correct SCDs could be retrieved for all trace gases at all retrieval wavelength range.

The necessary files to perform Test I for both measurement scenarios (see Sect. 3.2) are provided in the Supplement.

3.3.2 Test II: cross correlations of other absorbers with retrieved BrO SCD

Beyond studying the behaviour of retrieved trace gas SCDs with changing evaluation wavelength intervals, many other properties of a fit can be investigated (e.g. see Sect. 2). Test II is designed to yield information on the sensitivity of the retrieval to small variations in the amount of absorbers present. Cross correlations between the differential absorption cross sections of the different absorbers may affect the retrieved SCDs. Since the RCSs are wavelength dependent, these cross correlations depend on the retrieval wavelength range.

A series of fits were used to assess these cross correlations. The original sets of I_0-corrected RCSs were fit to synthetic spectra, which were constructed with varying strengths of absorbers. Dependencies of the retrieved BrO SCDs on other absorber strengths can be expressed as

$$\frac{\delta S_{\mathrm{BrO}}}{\delta S_{\mathrm{A}}} = \frac{S_{\mathrm{BrO,A+}} - S_{\mathrm{BrO,A-}}}{2\Delta S_{\mathrm{A}}} \cdot \left(\frac{S_{\mathrm{BrO,0}}}{S_{\mathrm{A,0}}}\right)^{-1}. \quad (3)$$

The derivative δS_{BrO} to variations in columns of absorber "A" (δS_{A}) is calculated from BrO SCDs $S_{\mathrm{BrO,A+}}$ and $S_{\mathrm{BrO,A-}}$, which are retrieved when changing the original SCDs of absorber A $S_{\mathrm{A,0}}$ by $\pm\Delta S_{\mathrm{A}}$, respectively. $S_{\mathrm{A,0}}$ and $S_{\mathrm{BrO,0}}$ are the SCDs as given in Table 2. The sensitivity of the BrO SCD at a certain retrieval wavelength range relative to changes in SCDs of all other absorbers is estimated by

$$\frac{\mathrm{d}S_{\mathrm{BrO}}}{\mathrm{d}S_{\mathrm{All}}} = \frac{1}{n_{\mathrm{A}}} \sum_{\mathrm{A}} \frac{\delta S_{\mathrm{BrO}}}{\delta S_{\mathrm{A}}} \quad (4)$$

where n_{A} denotes the total number of different absorbers excluding BrO.

An additional error is introduced by varying the absorbers while constructing the synthetic measurement spectrum without changing the I_0 correction of RCSs in the respective fit scenario. Thus the dependencies revealed are resulting from (1) cross correlations between different RCSs and (2) wrongly assumed trace gas SCDs when correcting for the I_0 effect of the respective trace gas.

The variations of the trace gases were set to 1 % for the measurement scenarios assessing stratospheric BrO by zenith-sky DOAS and 10 % for the measurement scenarios of BrO in volcanic plumes (see also Table 2). These choices are motivated by the different measurement conditions:

For the zenith-sky DOAS, changes in the measured trace gas SCDs are mainly induced by changes in SZA. The 1 % changes for the zenith DOAS scenario have been chosen, because they represent the mean deviation from the true O_3 SCDs observed in Aliwell et al. (2002), scenario B2 and C2 (see p. 4, Table 3), which correspond to the retrieval approach chosen in this publication. In case of the volcanic plume scenario, the motivation of 10 % deviations of true trace gas SCDs is that rapid changes of observed trace gas SCDs may occur due to changes in volcanic emission strength, which may well exceed 10 %. If aerosols or ash are present in the plume, also trace gas SCDs of the ambient atmosphere may vary due to different optical light paths observed.

Different trace gas SCDs may vary on a different scale, but for the sake of simplicity the same deviations were chosen for all trace gases in the respective measurement scenarios. For real measurement spectra, additional residual structures and noise may increase these cross correlations. Thus this test will only yield a "best-case" result.

3.3.3 Test III: effect of noise on retrieval and error calculation

In order to render the theoretical study more realistic, tests were performed on the synthetic spectra with added noise. Typical residual structures are simulated by adding Gaussian noise to the logarithm of the measurement spectra. The standard deviation of the noise structure was normalized to an optical density of 3×10^{-4}. Additional broad-band features were introduced by binomial low-pass filtering (e.g. Jähne, 2005) of the noise with 0, 10 and 50 iterations with subsequent rescaling (see Fig. 2). Iterations of 10 and 50 correspond to a filtering using a running mean of 6 and 15 pixels, similar to the error calculation study by Stutz and Platt (1996). A correction factor is defined in the study which is the ratio of standard deviation of results and the mean fit error. For one BrO absorption band with an average FWHM of 1.5 nm (15 pixels), the correction factor is ≈ 1.5 for unfiltered noise, ≈ 2.5–3 for noise filtered with 10 iterations and ≈ 4.5 for 50 iterations respectively.

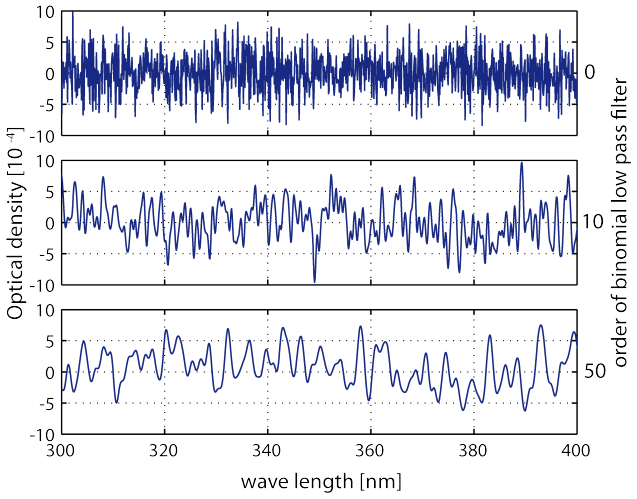

Fig. 2. Examples of different Gaussian noise spectra added to the logarithm of the synthetic spectrum. The broad-band structures are introduced by a low-pass filter using a binomial filter of 0 (top trace), 10 (center trace) and 50 (bottom trace) iterations respectively. After low-pass filtering, the noises were rescaled to the original standard deviation with an amplitude of 3×10^{-4}.

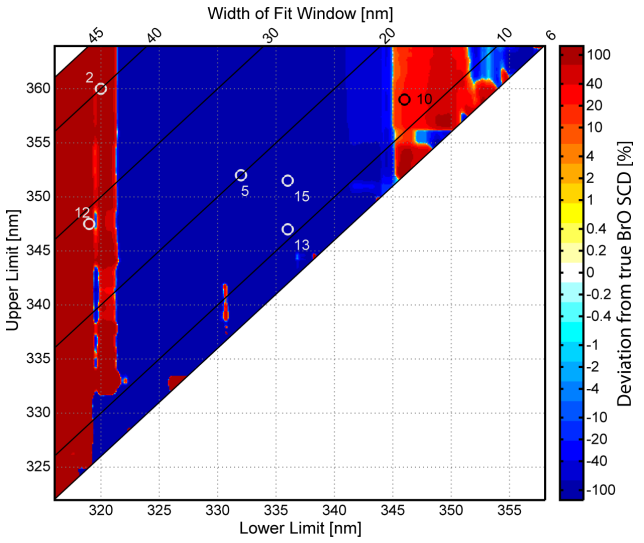

Fig. 3. Results from a retrieval wavelength mapping of a synthetic spectrum for the measurement scenario zenith-sky DOAS with a true BrO SCD of 1.5×10^{14} molec cm^{-2}. The plot shows a retrieval map constructed with the uncorrected RCSs used in the retrieval. Note that the colour code is on a logarithmic scale. Compared to the retrieval applying corrected RCSs (Fig. 1), highly erroneous SCDs are retrieved. The numbers denote certain wavelength intervals shown in Table 1.

The influence of noise on retrievals with I_0-corrected and uncorrected RCSs was tested for the case of unfiltered noise. Broader residual structures are studied only for I_0-corrected RCSs. In order to get reasonable statistics with independent retrieval results for each wavelength retrieval range, 100 maps with independent noise for each wavelength range are averaged to yield the presented retrieval maps.

4 Results and discussion of the individual measurement scenarios

Results of the different tests are presented in the following section, which were performed on the measurement scenarios of zenith-sky DOAS (see Sect. 4.1) and DOAS measurements of volcanic plumes (see Sect. 4.2).

4.1 Zenith-sky DOAS

4.1.1 Test I: influence of the I_0 effect on zenith-sky DOAS

Figures 1 and 3 depict the deviation from the true BrO SCD of 1.5×10^{14} molec cm^{-2} for I_0-corrected and uncorrected RCSs used in the retrieval, respectively. In the case of I_0-corrected RCSs (see Fig. 1), retrieved BrO SCDs vary by more than 10 % at most retrieval ranges including wavelengths below 330 nm. If fits are only performed at longer wavelengths, deviations of less than 1 % are achieved for lower limits $>$ 345 nm. Note that no additional residual structures or noise has been added in this test, and therefore the results can be regarded as a lower limit of accuracy.

If uncorrected RCSs are applied in the fitting algorithm (Fig. 3), the retrieval of the true BrO SCD is not unambiguously possible. Highly erroneous results by more than 100 % are to be expected for retrieval wavelength intervals including wavelengths below $\approx$ 340 nm. Even at longer wavelengths, most wavelength intervals yield SCDs deviating by more than 20 % from the true BrO SCD.

For both sets of RCSs, one of the major features visible in the retrieval maps is that the results depend mostly on the lower wavelength limit. This indicates the influence of the strong O_3 absorptions, because their absorption structures decrease with increasing wavelength. Preferences to under- or overestimate the true BrO SCD change with the BrO absorption maxima included in the retrieval wavelength interval.

Figure 4 depicts retrieval results and residuals at three different wavelength ranges for uncorrected and I_0-corrected RCSs. The evaluation wavelength intervals chosen correspond to the ones marked by #12 (319–347.5 nm), #5 (332–352 nm) and #10 (346–359 nm) in Table 1, Figs. 1 and 3. Greater residual structures occurring for the retrieval between 319 nm and 347.5 nm confirm that retrievals at lower wavelength ranges and the use of uncorrected RCSs must be avoided if higher O_3 absorptions are present in the measurement spectra, even in this "best case" using synthetic spectra without noise. The residuals of the retrievals using other wavelength intervals aside from 346–359 nm still show strong residual structures if I_0-corrected RCSs are applied in

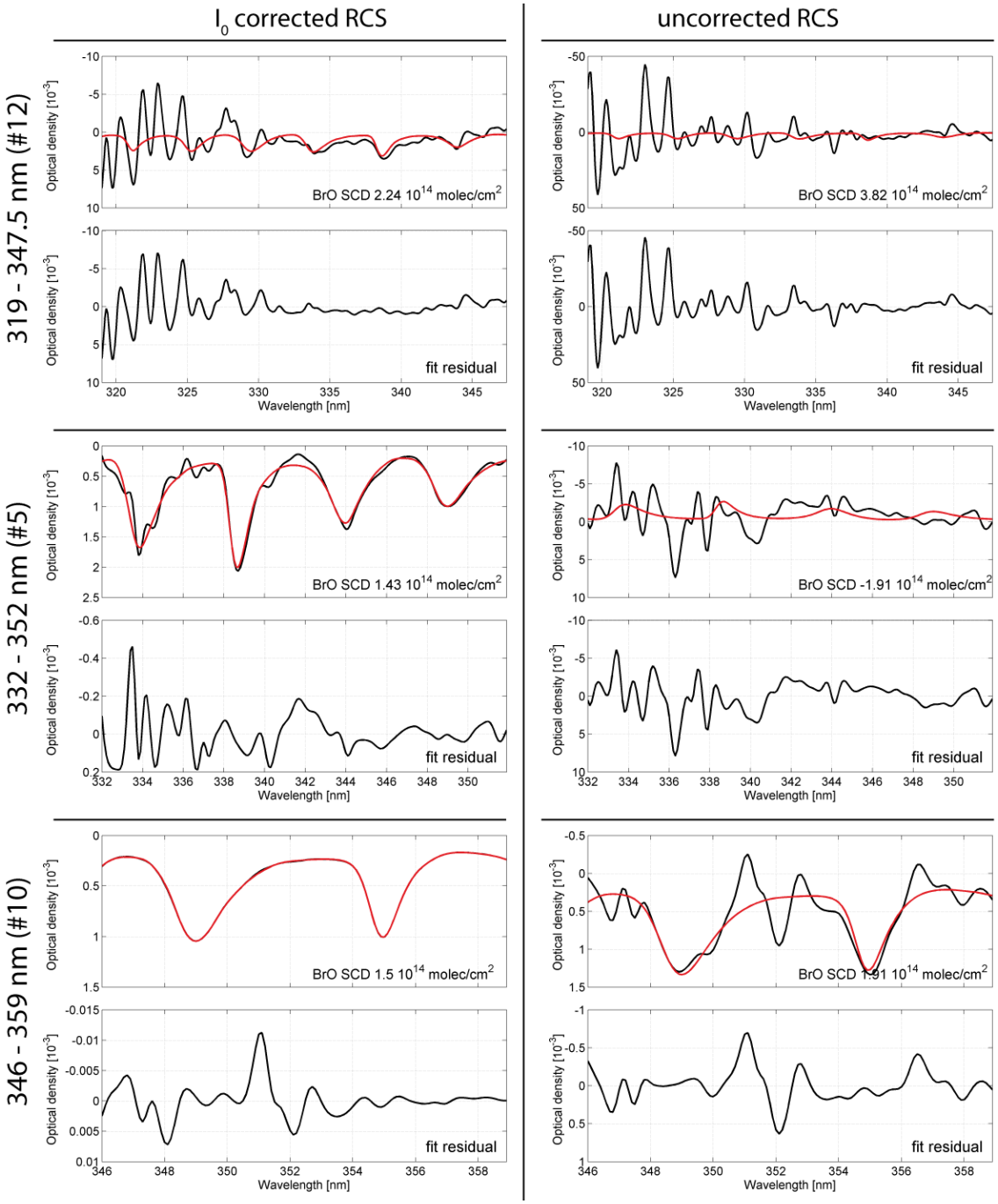

Fig. 4. Shown above are fit results of the measurement scenario zenith-sky DOAS for three different wavelength intervals, corresponding to #12, #5 and #10 in Table 1. The fit of the BrO RCS and the residuum are displayed. Left column: uncorrected RCSs; right column: I_0-corrected RCSs. Regardless of which RCSs are used, a fit applying the longest wavelengths (346–359 nm) yields the most accurate results. At 346–359 nm, tests C1 and C2 on synthetic spectra in Aliwell et al. (2002) are reproduced.

the fitting process. The residual structures of the retrieval using uncorrected RCSs at 346–359 nm reproduce the results of tests C1 and C2 described in Aliwell et al. (2002), both in retrieved BrO SCDs and shapes of the residual.

4.1.2 Test II: cross correlations of other absorbers for zenith-sky DOAS

In this test, the dependencies of the retrieved column density of the trace gas of interest (i.e. BrO) on changes in other

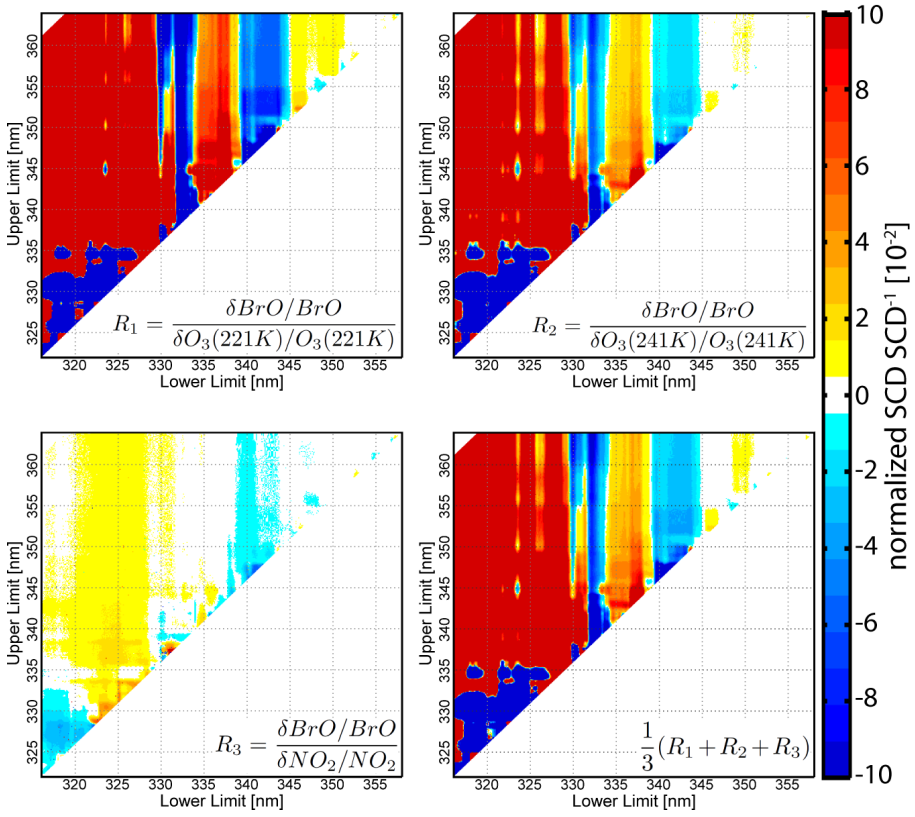

Fig. 5. Cross correlation study for the zenith-sky DOAS scenario. Changes in BrO SCDs if potentially cross correlating absorbers are varied by 1 %. The colour code depicts relative changes of the retrieved BrO SCD per relative change of absorber. At shorter wavelengths, the strong O_3 absorptions are clearly dominating (upper row), whereas the influence of NO_2 is negligible in comparison (lower left). The average of all relative changes is depicted in the lower right graph.

absorber strengths were investigated. Figure 5 depicts the relative change in retrieved BrO SCD when varying the strength of the other absorbers in the synthetic measurement spectrum by 1 %. If any of the O_3 RCSs are varied by 1 %, a relative change of BrO of more than 10 % occurs for wavelength ranges with a lower limit between 316–330 nm. Even above a lower wavelength interval limit of 330 nm, changes of BrO SCDs greater than 10 % are present for O_3 at 221 K, the stronger of the two O_3 RCSs used. Relative changes of BrO SCD due to O_3 at 241 K remain mostly below 5 % above a lower limit of $\approx$ 335 nm and become negligible above 345 nm. Therefore, the variations of SCDs for the zenith-sky DOAS scenario show a clear imprint of the strong O_3 absorptions. They generally lead to an overestimation of BrO SCDs if wavelengths $<$ 330 nm are included in the retrieval. The strong O_3 absorptions also affect the retrieved BrO SCDs at longer wavelengths, although not as severely.

Compared to O_3, the influence of varying the NO_2 SCD is only minor and can be disregarded when evaluating at intervals starting above a lower limit of 345 nm. However, the depicted dependency of NO_2 at the shorter wavelength end of the evaluation range is surprising. Other than O_3, the differential optical absorption bands of NO_2 increase in strength towards longer wavelengths. Thus, a dependency on the upper wavelength end of the evaluation retrieval would be expected (see also Sect. 5.2).

4.1.3 Test III: effect of noise on retrieval and error calculation for zenith-sky DOAS

Figure 6 depicts the retrieved BrO SCDs if additional noise structures are added to the synthetic spectra. A sample of the different noises is shown in Fig. 2. Comparing the retrieved BrO SCDs from synthetic spectra without (Test I) and with unstructured noise, the mean BrO SCDs of the noisy spectra do not differ from the ones without noise, regardless of whether the RCSs are corrected for the I_0 effect or not (Figs. 1, 3). With an increase in noise structure (column 2 till 5), an increase in standard deviation of results is observed. The variations observed in Figs. 1 and 3 are also more apparent with increasingly structured noise. Whereas the average BrO SCDs around a lower retrieval wavelength limit of 332.5 nm for all upper limits (thus following a vertical line) do not deviate from the results of synthetic spectra without noise, the average of the retrieval starts to systematically underestimate the results with increasing noise

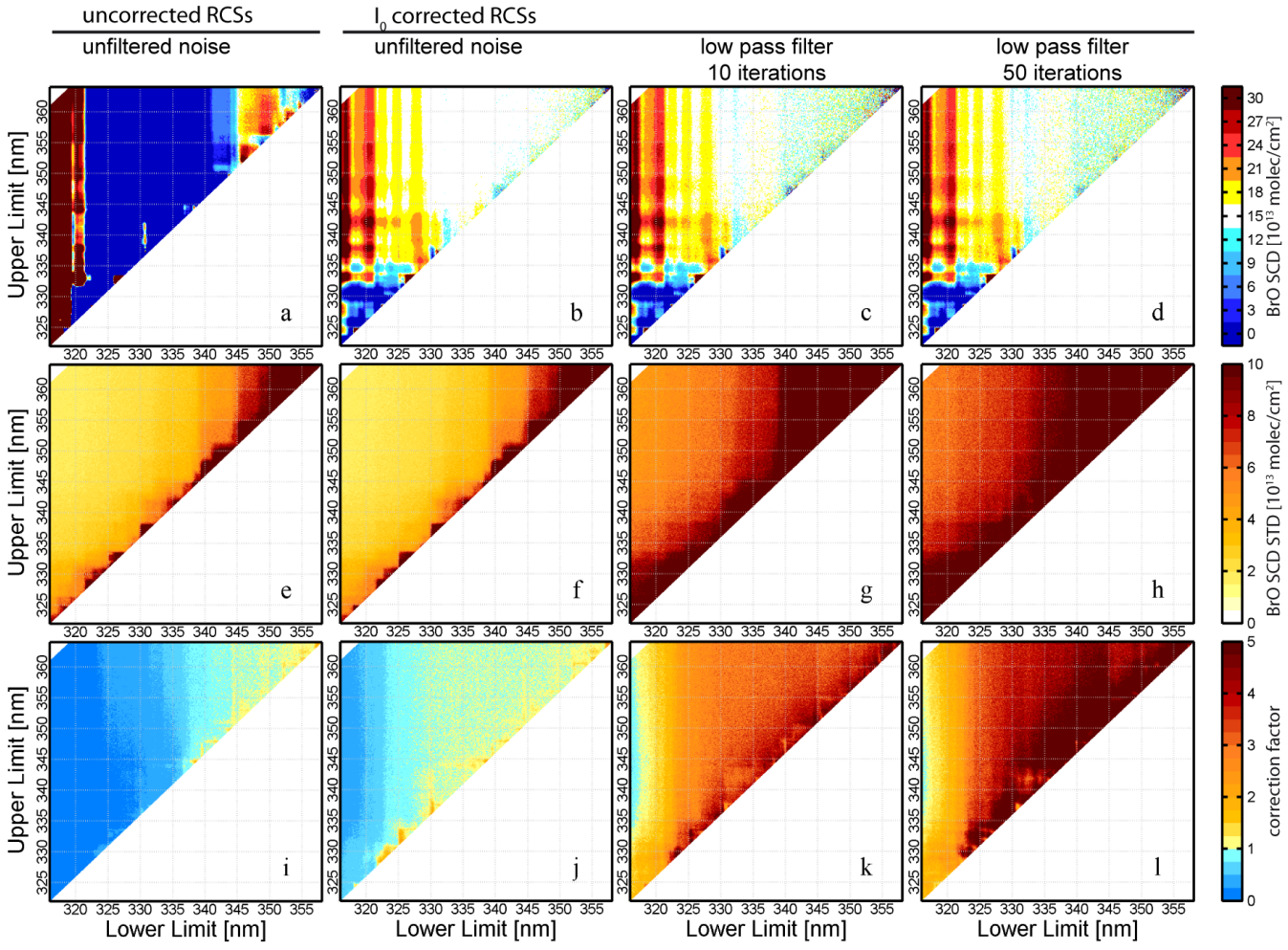

Fig. 6. Results from the statistical study on the zenith-sky DOAS measurement scenario. For information on the noises applied to the synthetic spectra, the reader should refer to Sect. 3.3.3. The first column shows results for an uncorrected set of RCSs together with unfiltered noise. The second till fourth column depict results for I_0-corrected RCSs and different filtered noises. The rows (upper to lower) correspond to retrieved SCDs, standard deviation of results, and calculated correction factors defined as the standard deviation divided by the fit error (top to bottom row, respectively).

structure. The same is true for an overestimation of SCDs between lower limits of 334–338 nm. This indicates that underlying systematic errors are not concealed by noise but actually become more pronounced. The reason for this is yet unclear.

The standard deviation shows a clear change at ≈ 338 nm, 345 nm and 350 nm of lower limit of the retrieval interval for all cases studied (different noise types, uncorrected and I_0-corrected RCS). These changes correspond to the maxima of different BrO absorption bands included in the fitting process. Comparing standard deviations of uncorrected and I_0-corrected RCS, no major difference can be observed. Therefore, the unstructured noise does not obviously influence the distribution of retrieved SCDs even if systematic structures are present. Nevertheless, the systematic structures influence the fit error greatly. This can be observed in Fig. 6 by looking at the correction factor, the ratio between standard deviation and fit error (see Sect. 3.3). For unfiltered noise, a correction factor below 1 is calculated for evaluations of lower limit < 330 nm for I_0-corrected RCS, and even a factor below 1 for all evaluations of lower limit < 345 nm for uncorrected RCS. A possible reason for this behaviour is discussed in Sect. 5.

4.2 BrO in volcanic plumes

4.2.1 Test I: influence of the I_0 effect on retrievals of BrO in volcanic plumes

Figure 7 shows the results for the measurement scenario of BrO in volcanic plumes for a retrieval using I_0-corrected RCSs. It is apparent that the I_0-corrected retrieval yields results with only minor deviations from the true BrO SCD at

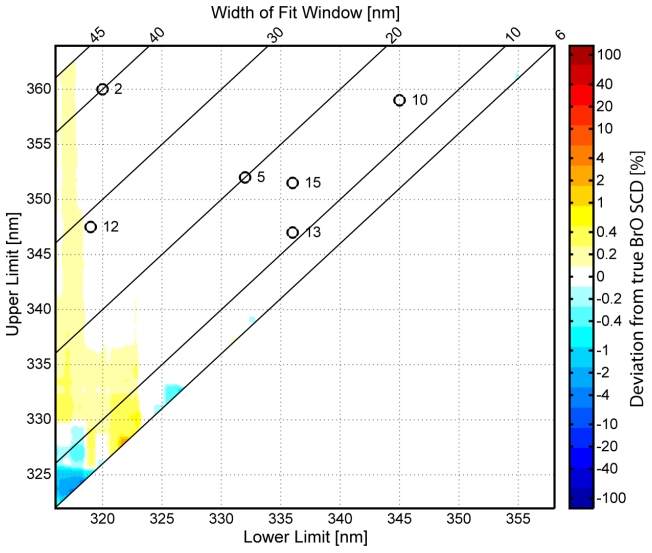

Fig. 7. Deviations from the true BrO SCD (1.5×10^{14} molec cm^{-2}) for the measurement scenario of BrO in volcanic plumes using I_0-corrected RCS. The retrievals only show minor structures if lower wavelengths are included in the fit. The numbers indicate the different retrieval ranges in Table 1.

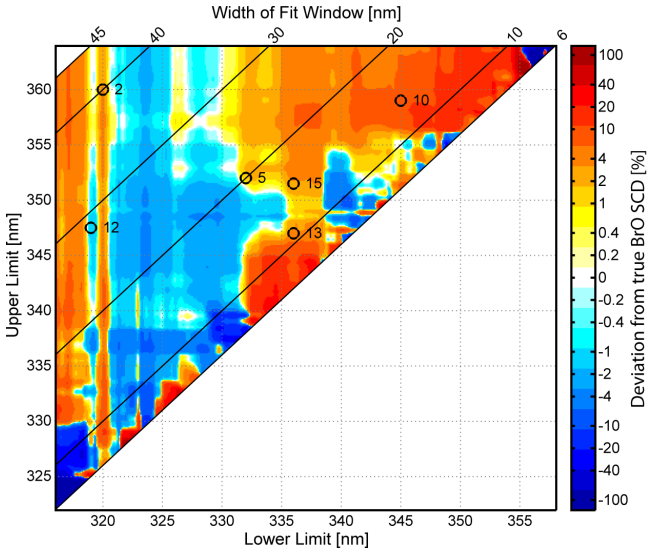

Fig. 8. Deviations from the true BrO SCDs in the measurement scenario of volcanic plumes applying uncorrected RCSs in the retrieval. Over- or underestimation of the target BrO SCD of 1.5×10^{14} molec cm^{-2} is higher compared to I_0-corrected RCS (Fig. 7). Retrievals at longer wavelength ranges (> 345 nm) systematically overestimate the BrO SCD. The index numbers denote selected wavelength intervals from Table 1.

most evaluation wavelength intervals. The deviations range up to 1 % only if the fit is performed with a retrieval interval including wavelengths below ≈ 323 nm. These features may be attributed to the stronger SO_2 and O_3 absorptions at shorter wavelengths. Also residual structures shown for three different evaluation wavelength ranges are negligible (Fig. 9).

If uncorrected RCSs are used, the retrieved BrO SCDs show larger deviations from the true BrO SCD (Fig. 8), however far less than observed in the scenario for zenith-sky DOAS (Fig. 3). In general, a systemic overestimation of BrO SCDs is apparent if lower wavelength limits below 319 nm and above 332.5 nm are included in the retrieval; otherwise, BrO SCDs are slightly underestimated. Deviations from the true BrO SCD range of more than 10 % are only observed at lower limits > 347.5 nm and in the range of lower limits > 332.5 nm, < 340 nm, upper limits < 345 nm for upper limits < 330 nm.

Assigning deviations at a specific retrieval wavelength range to a certain trace gas is difficult since possible cross correlations may occur between all trace gases. Also, changes in retrieved SCDs of absorbers do not directly translate into the same changes in the respective optical density of the differential optical absorption structure due to the wavelength dependency of the RCSs. As an example, optical densities are given in Table 3 for different trace gases at three different wavelengths. An attempt to assign different wavelength intervals to the different absorbers that interfere the most with the BrO retrieval at respective wavelength ranges is presented in Appendix A. It indicates that the observed deviations from the true BrO SCD in Fig. 8 may be caused by cross correlations between the RCSs of BrO and HCHO.

Figure 9 displays fit examples for uncorrected and I_0-corrected RCSs. As expected from the previously shown Figs. 7 and 8, only small residual structures and deviations from the true BrO SCD are observed. For the retrievals applying I_0-corrected RCSs, all three different retrieval wavelength ranges yield negligible residual structures. In contrast to the fit examples of the zenith-sky DOAS scenario (Fig. 4), the retrieval wavelength interval between 332 nm and 352 nm is most accurate and the wavelength interval of 346–359 nm shows the largest deviation from the true BrO SCD.

4.2.2 Test II: cross correlations of other absorbers when evaluating BrO in volcanic plumes

As described in the previous paragraph, I_0-corrected RCSs yield accurate results with only slight deviations from the true BrO SCD when lower wavelengths are included ($<$ 325 nm, Fig. 7). These results are also confirmed when varying the strengths of other absorbers in the case of the scenario for volcanic plumes. The influence of changes in other absorber strength on the retrieved BrO columns is visible for I_0-corrected RCSs in Fig. 10. The increased absorptions of O_3 and SO_2 below 325 nm lead to a small overestimation of BrO SCDs if these wavelengths are included in the retrieval wavelength interval. In the case of NO_2, almost all wavelength intervals show an anti-correlation with BrO. The absorption structure of NO_2 is rather complex and does not

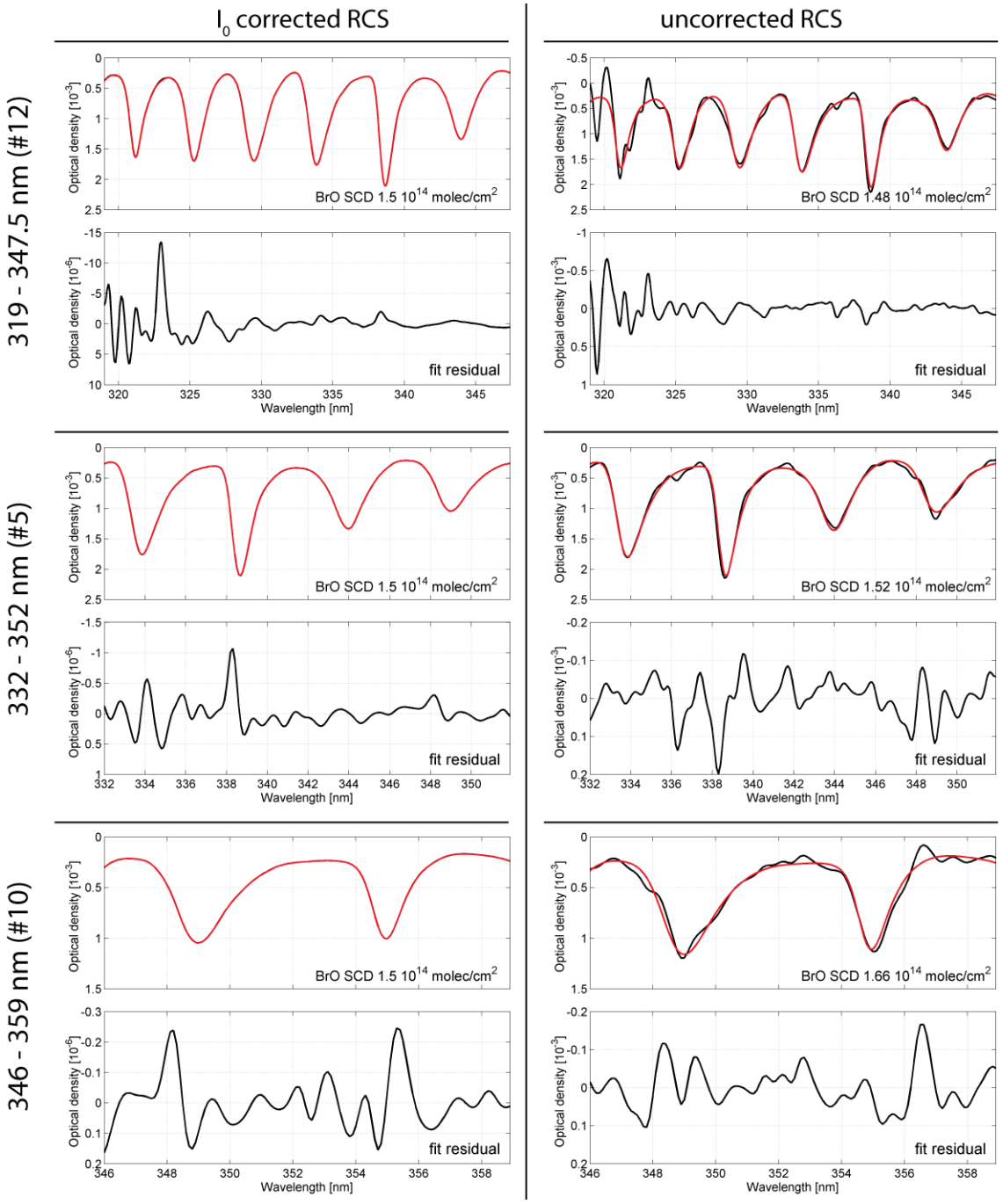

Fig. 9. Fit examples for selected wavelength intervals (#12, #5, #10 in Table 1) for the measurement scenario of BrO in volcanic plumes: all wavelength intervals yield results with negligible residual structures applying I_0-corrected RCSs. For fits applying uncorrected RCSs, the largest deviation is seen for the interval of 346–359 nm (#10) in contrast to the scenario of zenith-sky DOAS (Fig. 4). Note that the optical density for the fit residual is given in units of 10^{-6} for I_0-corrected RCSs and in units of 10^{-3} for uncorrected RCSs.

show clearly overlapping absorption bands with BrO. Nevertheless, NO_2 interacts unfavourably with BrO due to its comparably high optical density (Table 3). BrO shows the least dependency on changes in absorber strength to HCHO. Cross correlations are mainly observed at shorter wavelength limits between 335–340 nm and above 345 nm. This may be attributed to absorption bands of similar shape for both trace gases at $\approx$ 338 nm.

The average of all dependencies in Fig. 10 is shown in Fig. 11. BrO SCDs obtained in retrieval wavelength intervals

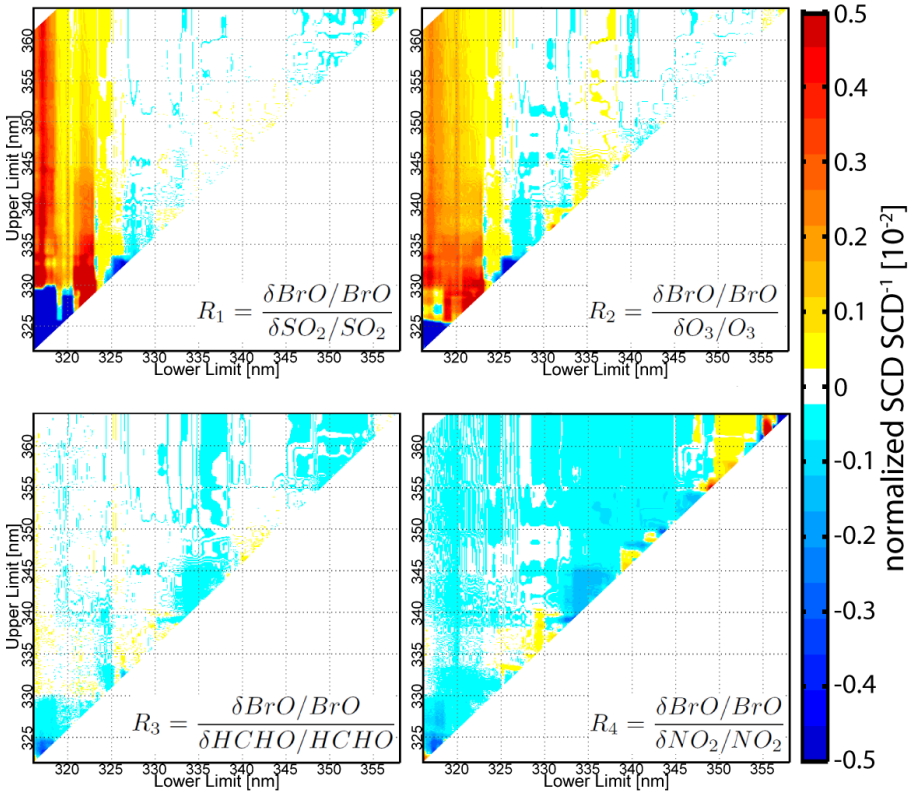

Fig. 10. The plots depict the influence of varying absorber strength on the retrieval of BrO in volcanic plumes. Retrieval wavelength maps are constructed using absorber strengths varied by 10 %. The original I_0-corrected set of RCSs was used. Greatest deviations from the true BrO SCD occur where strong absorption features of SO_2 or O_3 are included (e.g. at evaluation ranges including wavelengths ≤ 323 nm). While these effects correlated to the BrO SCDs, NO_2 and HCHO mostly anti-correlate with BrO, of which the first shows greater influence.

Table 3. Differential optical densities of trace gases at SCDs applied in the measurement scenarios of BrO in volcanic plumes. The differential optical densities are calculated by taking the peak to peak value of a high-pass filtered absorption cross section multiplied by the respective SCD in a 5-nm wavelength interval. The 325-nm and 350-nm wavelengths were chosen to indicate approximate optical densities in the lower and higher wavelength ranges. The strongest absorption band of BrO is situated at ≈ 338 nm.

Center of wavelength interval	BrO	SO_2	O_3	NO_2	HCHO
[nm]	optical density $\left[10^{-3}\right]$				
325	0.7	6.2	5.0	0.7	1.0
338	1.2	0.1	1.2	2.0	0.7
350	0.3	0.1	0.1	3.5	0.2

with a lower limit < 325 nm are dominated by O_3 and SO_2, whereas results at other wavelength intervals may be influenced mainly by NO_2 and HCHO. The area least affected by varying absorber strengths is observed between the lower limits of 326 nm and 333 nm. However, cross correlations in total remain negligible as long as the stronger differential absorption structures of SO_2 and O_3 are avoided.

4.2.3 Test III: the effect of noise on retrieval and error calculation for BrO in volcanic plumes

The effects of different noise spectra on the retrieval of BrO in volcanic plumes are depicted in Fig. 12. As already observed for the scenario of zenith-sky DOAS (Sect. 4.1.3), BrO SCDs are comparable to evaluations without noise (see Figs. 7, 8). Possible minor deviations from the true BrO SCDs for evaluations applying I_0-corrected RCSs are still concealed by the noise. Comparing the standard deviations for retrievals using uncorrected and I_0-corrected

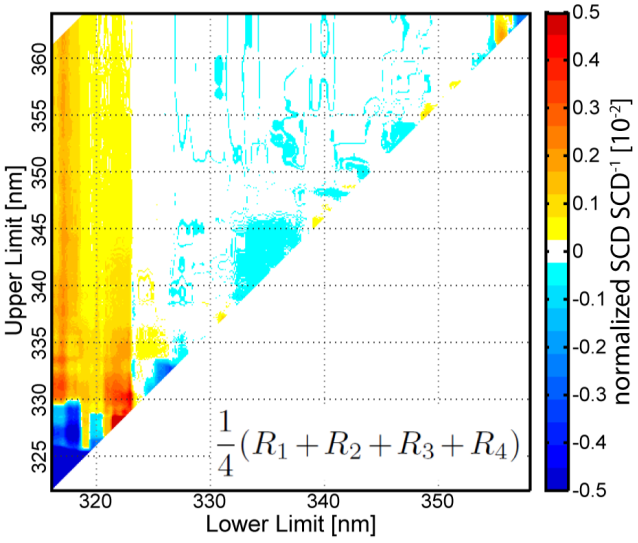

Fig. 11. The figure depicts the average of cross correlations of other trace gases with the BrO retrieval (Fig. 7). Wavelength evaluation ranges with a lower limit < 325 are dominated by O_3 and SO_2 features, whereas the other wavelength ranges may be influenced mainly by NO_2 and HCHO.

RCSs (Fig. 12e, f), no differences can be distinguished, although results for both types of evaluations differ (Fig. 12a, b). Therefore, the unfiltered noise leads to comparable standard deviation of retrieved BrO SCDs, but absolute results are dominated by the underlying systematic residuals. In the case of the I_0-corrected RCSs, the average SCDs remain the same, independent of the different filtered noise spectra. A general increase in standard deviation is visible with an increase in structure of the noise spectra (i.e. stronger low-pass filtering). For all types of noise spectra, a sudden increase in standard deviation occurs at shorter retrieval wavelength limits of 338 nm and 345 nm, corresponding to the maxima and decrease in amplitude of the differential optical absorption bands of BrO included in the fit.

The calculated correction factor shows a clear transition at a lower limit of 320 nm for uncorrected RCSs, changing from below unity to an average value of 1 for all other retrieval wavelength intervals. For I_0-corrected RCSs, the correction factor only shows a small wavelength dependence. For unfiltered noise, standard deviation and measurement error do not differ significantly. For low-pass filtered noise, correction factors of ≈ 3 and ≈ 4.5 (10 and 50 iterations of the binomial filter, respectively) need to be applied to calculate the true standard deviation from the fit error.

5 Comparison of results from both measurement scenarios

The three tests for both measurement scenarios yield several common features. Even if generalisations are difficult without a thorough mathematical description, these findings offer empirical insights and reveal common pitfalls in DOAS evaluations.

5.1 I_0-corrected and uncorrected reference cross sections

Although the two measurement scenarios incorporate absorptions of differing strengths, retrieved SCDs showed that an I_0 correction should always be applied. This is especially true if very strong absorbers conceal the trace gas of interest (e.g. O_3 concealing BrO in the scenario zenith-sky DOAS scenario). Even in this best-case study, an insufficient correction of the I_0 effect yielded deviations of the BrO SCDs at lower wavelengths with high O_3 absorptions. In the case of the scenario of BrO in volcanic plumes, the combined SO_2 and O_3 differential absorptions are still about two orders of magnitude smaller than the combined O_3 differential absorptions in the zenith-sky DOAS scenario at wavelengths ≥ 320 nm. Therefore, deviations of the retrieved BrO SCDs are much smaller than for the zenith-sky DOAS scenario. Nevertheless, I_0 correction of the RCSs remains mandatory to achieve correct results.

The observed deviations when using I_0-corrected RCSs can be attributed to a slightly erroneous correction of the I_0 effect since the denominator in the correction (Eq. 2) consists only of the incident solar light without the presence of other absorbers. Sensitivity tests were performed with true I_0-corrected RCSs as outlined in Sect. (3.1). Using these sets of RCSs, true SCDs of all trace gases could be retrieved at all wavelength intervals for both measurement scenarios.

5.2 Sensitivity to cross correlating absorbers

In both measurement scenarios, variations in the strengths of other absorbers affected the BrO retrieval. These errors in the retrieved BrO SCDs are due to a combination of cross correlations between the different absorbers and an I_0 correction of RCSs with slightly erroneous SCDs. The observed dependencies are up to two magnitudes greater for the zenith-sky DOAS scenario than for the measurement scenario of volcanic plumes. Since the contributions of cross correlations and I_0 correction have not been separated, it is not possible to assign observed dependencies clearly. However, the observed correlations are in general quite small. Since (1) the synthetic spectra in this test are constructed without noise or other wavelength-dependent residual structures and (2) the retrieval wavelength ranges studied are sufficiently large at > 60 channels of the simulated detector, a precise retrieval of all absorbers should be possible. The only sources of error remaining are malicious spectral features induced by the insufficient I_0 correction of RCSs. This hypothesis is strengthened by the observations for the zenith-DOAS measurement scenario (Fig. 5). The similarities of the structures observed for variations of O_3 and NO_2 SCDs indicate that the structures

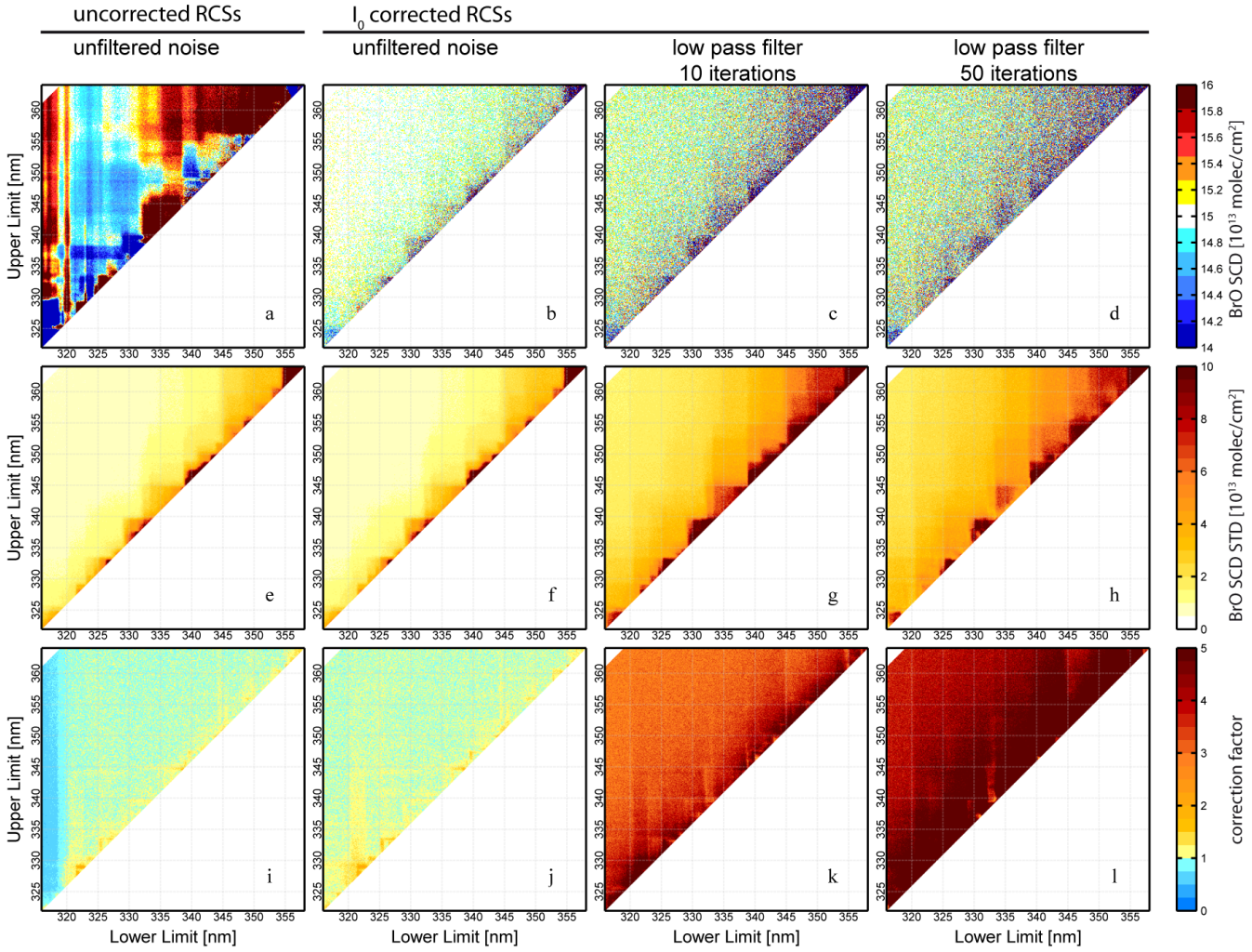

Fig. 12. The graph depicts results of the the statistical study for the scenario of measuring BrO in volcanic plumes. Different types of noise spectra were added to the logarithm of the synthetic spectra (see Sect. 3.3.3). The first column shows results for unfiltered noise and an uncorrected set of RCSs applied in the fit. In the second, third and fourth column, results are plotted for I_0-corrected RCSs applied to synthetic spectra with unfiltered noise and low-pass filtered noise. The mean BrO SCDs retrieved are shown in the top row; the middle row depicts the standard deviation of SCDs and the bottom row the calculated error correction coefficient.

observed in the NO_2 plot may originate from the insufficient correction of the I_0 effect of the O_3 RCSs.

Thus for the case of measured spectra, it can be speculated that retrieval wavelength interval-dependent correlations between trace gases originate from systematic residual structures. One such example is the anti-correlation between BrO and HCHO observed in measurements of volcanic plumes (Vogel, 2011), which occur despite the negligible correlations described in Sect. 4.2.2 and only minor anti-correlations found in Appendix A. For field measurements of volcanic plumes, systematic spectral structures are likely induced by wavelength-dependent radiative transfer effects, which are not fully considered in a standard DOAS retrieval.

5.3 Influence of noise on the retrieval

In Sects. 4.1.3 and 4.2.3, the influence of noise on the DOAS retrieval was tested. For both scenarios, SCDs obtained from synthetic spectra without additional noise were comparable to the mean of retrieved SCDs of spectra with noise. These findings also remained true in general when noise spectra were calculated with additional, random broad-band structures. However, the deviations from the true BrO SCD were slightly increased with increasing broad-band structures of the noise in the case of the zenith-sky DOAS scenario for reasons yet unclear.

The relationship between standard deviation of retrieved SCDs, fit error and the correction factor used to calculate one from the other has been described in Stutz and Platt (1996).

They found that the true standard deviation of retrieved SCDs is always larger than the fit error. However, the authors assumed that no systematic residual structures were present. The results presented in Sects. 4.1.3 and 4.2.3 reveal several interesting features. (1) Comparing results from retrievals applying uncorrected and I_0-corrected RCSs, it can be seen that the standard deviation of the retrieved SCDs does not appear to depend on systematic wavelength structures due to the I_0 effect. (2) However, the increase of the fit error by these systematic structures may lead to a correction factor < 1. Therefore, the application of a correction factor may lead to overestimation of the true standard deviation.

The observed effects are not pronounced when systematic residual structures are small, and thus the boundary conditions of the previous study are fulfilled. In that case, the correction factor calculated for the BrO retrieval corresponds to the previously published approach. It is only dependent on the width of the differential absorption structure and width of the residual features, here ≈ 1.5 for unfiltered noise, ≈ 2.5–3 for noise filtered with 10 iterations and ≈ 4.5 for 50 iterations.

To perform an extensive error analysis on a theoretical basis is beyond the scope of this work. However, based on the empirical studies performed here, we conclude that correction factors calculated assuming only random structures should also be applied if systematic residual structures are present. This approach may lead to an overestimation of the standard deviation of results, but the systematic spectral structures will also lead to a systematic offset of the average retrieved columns.

5.4 Recommended retrieval wavelength intervals

For zenith-sky DOAS, the tests confirmed the evaluation wavelength range 346–359 nm as suggested by Aliwell et al. (2002) due to greater stability of retrieved SCDs in measured spectra in comparison to 345–359 nm. If one compares this explanation with Fig. 1, it may be speculated that the observations may have been induced by shifts in the wavelength to pixel mapping of the spectrograph. The retrieval wavelength maps show a strong gradient for the 345–359 nm range, which is not present for 346–359 nm. At this known example, the novel tool confirms that this retrieval wavelength interval of BrO offers at least the dependency on the I_0 effect, although an I_0 correction of RCSs is still mandatory. BrO retrievals including lower wavelengths are not advised since strong O_3 absorption and slightly insufficient I_0 correction of RCSs may yield highly erroneous columns even in this "best-case" scenario.

BrO retrievals for measurement of volcanic plumes show a much lower I_0 dependency of the BrO SCDs on the retrieval wavelength interval, mostly due to a total O_3 SCD that is about 100 times weaker. Whereas the fit applying I_0-corrected RCSs shows a good agreement with the true BrO SCD at most wavelengths, BrO SCDs retrieved with uncorrected RCSs can differ by more than 10 %. In the field, volcanic emissions can vary greatly on short time scales. Also, changing O_3 SCDs in early and late hours of the day have to be considered. Therefore, a retrieval wavelength range with a low dependency on the I_0 effect and cross correlations to other absorbers is needed rather than one that can be well corrected under stable conditions. In an evaluation wavelength range with a lower limit between 320–335 nm, the deviations from the true BrO SCDs are below 5 % applying uncorrected RCSs. Given the variability of strong absorbers at lower wavelengths, i.e. SO_2 and O_3, and the increased cross correlations observed for lower wavelength limits < 325 nm (Sect. 4.2.2), evaluations should be performed at the upper range of suggested interval.

However, a specific retrieval wavelength interval can not be recommended for the evaluation of BrO in volcanic plumes here. Advanced modelling of synthetic spectra (including realistic simulations of the atmospheric radiative transfer and the Ring effect in a 3-dimensional atmosphere once the respective tools are created) in comparison with measured spectra is needed in order to advise one on choosing a specific retrieval wavelength interval. A simplified approach is presented in Appendix B, but the results need to treated with care for the above given reasons.

6 Conclusions

The retrieval wavelength interval is one of the most important parameters in a DOAS retrieval. Finding the optimal retrieval wavelength interval is not trivial, because many wavelength-dependent effects may influence the retrieval, such as instrumental features, cross correlations between absorption cross sections and wavelength-dependent radiative transfer. Previous publications were motivated by the comparison of the applied wavelength retrieval interval with typically one or two additional wavelength intervals. The lack of appropriate visualisation prohibited a systematic study of the parameter space and made an easy determination of the optical retrieval wavelength interval extremely difficult.

In this study a novel method is presented that consists of systematically varying the retrieval wavelength interval of DOAS retrievals and displaying the results in a contour plot. In this way, appropriate spectral intervals become immediately visible. Furthermore, the method is not limited by studying the dependency of the retrieved SCDs on the evaluation wavelength intervals. Other parameters influencing the DOAS retrieval can be studied in the same way, such as cross correlations of RCSs, the effect of errors in the I_0 correction, residual amplitude and shifts in wavelength-pixel calibration of the instrument.

In order to prove the concept, several tests were performed for two synthetic measurement scenarios of BrO by passive DOAS instruments. The scenario for zenith-sky DOAS reproduces conditions of stratospheric BrO measurements

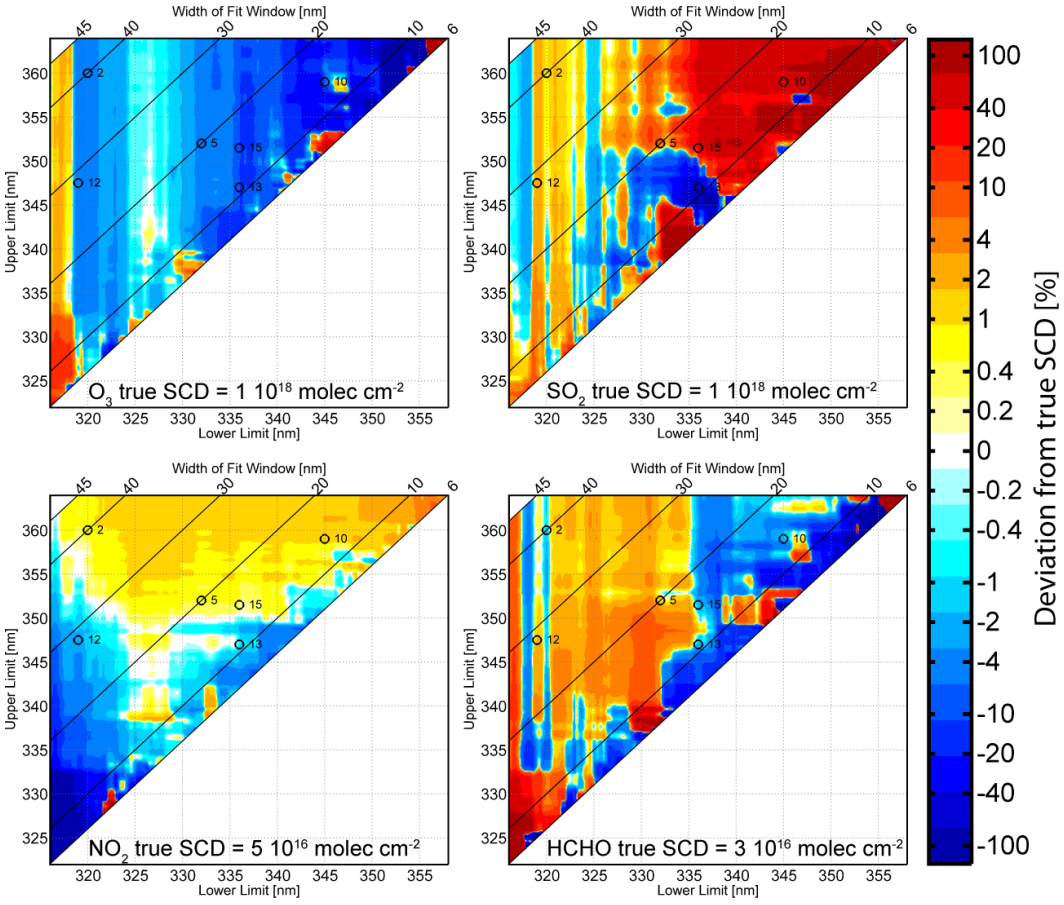

Fig. A1 Deviations from the true SCDs of trace gases other than BrO in test I of the measurement scenario of BrO in volcanic plumes using uncorrected RCSs. The respective true SCD ±1 % is indicated in white, over- and underestimation in red and blue colours.

at mid-latitudes, whereas the scenario of BrO in volcanic plumes captures typical conditions encountered when measuring BrO in tropospheric volcanic plumes. For the latter measurement scenario, this work constitutes the first systematic study of the dependency of retrieved BrO SCD on the retrieval wavelength interval. Tests on synthetic spectra included the assessment of the I_0 effect and the influence of its correction on the BrO retrieval. Furthermore, cross correlations between different absorption cross sections were investigated and a statistical study was conducted on the influence of noise on the retrieval.

By studying synthetic spectra, interpretation of results is aided by knowledge of the SCDs applied to construct the spectra. Measured spectra usually lack this a priori knowledge, and thus other approaches have to be chosen to obtain an optimal retrieval wavelength interval. For example, for certain measurement conditions some trace gases should not be present. In the case of MAX-DOAS measurements, different reference spectra can be compared, whereas nighttime measurements of LP-DOAS systems should not yield BrO or other photochemically produced species.

For the example of synthetic spectra of passive DOAS measurements, the novel tool of retrieval wavelength mapping was introduced. However, the method is not limited to these types of instruments but can be applied to any DOAS measurement. Thus, it enables a systematic study of important retrieval parameters, can highlight pitfalls in any DOAS retrieval and allows for an encompassing motivation of applied parameters.

Appendix A

BrO in volcanic plumes – Test I: individual SCDs of all trace gases applying uncorrected RCSs

In Sect. 4.2.1 results of the retrieval using corrected and uncorrected RCSs are discussed. Here, an attempt is made to assign the observed deviations of retrieved BrO SCDs to individual trace gas absorptions present in the synthetic spectrum. Since the deviations for the retrieval using I_0-corrected

RCSs are negligible, the discussion is restricted to the retrieval applying uncorrected RCSs.

Table 3 shows the differential optical densities of all trace gases in the synthetic spectrum for three different wavelength intervals. These values serve as indications for the influence of the respective trace gas at these wavelengths. The individual retrieval results for trace gases other than BrO are depicted in Fig. 5.4. Their respective true SCD in the range of $\pm 1\,\%$ is denoted in white. Deviations will influence the retrieval as a whole. In combination with the respective optical density, it indicates the influence of the respective trace gas to erroneous retrieval results in general.

SO_2 and O_3 absorptions influence the retrieval of BrO if shorter wavelengths (< 325 nm) are included in the retrieval wavelength interval, although by far not as strong as in the case of the scenario zenith-sky DOAS. Due to the overall decrease in absorption cross sections with longer wavelengths for both species, their influence is reduced at longer wavelengths. However, the optical density of O_3 is still comparable to the one of BrO at 338 nm. Strongly deviating SCDs are retrieved for SO_2 above 335 nm (Fig. 5.4), but its optical density at these wavelengths is negligible compared to other absorbers. If the retrieval includes longer wavelengths ($>\approx$355 nm), it can be assumed that errors due to NO_2 become more pronounced since its differential optical density increases and an overestimation of SCDs occurs (see Fig. 5.4).

The absorption bands of HCHO have a shape very similar to BrO, which may lead to an anti-correlation of both trace gases. On the one hand, the overestimation of HCHO SCDs for evaluation intervals starting at a lower limit (approximately 320–335 nm) might decrease retrieved BrO SCDs in that area. On the other hand, underestimation of HCHO SCDs at lower limits > 335 nm can increase BrO SCDs. These findings are reflected in Fig. 7, where BrO SCDs are generally below the true column in evaluation regions of a lower limit range between 320 nm to 335 nm and above for lower limits greater than 335 nm. Especially, overestimations of HCHO SCDs at a lower wavelength limit of 327.5–332 nm and upper limit of < 350 nm correspond to underestimated BrO SCDs (Fig. 8). These results indicate that BrO–HCHO cross correlations may cause erroneous retrieval results under similar measurement conditions. However, since the deviations of BrO SCDs are a result of a combination of all trace gas cross correlations, it is not unambiguously possible to assign deviations in the retrieved BrO SCDs to an individual trace gas alone.

Appendix B

Influence of the Ring effect

In this appendix, an attempt to assess the influence of the Ring effect is made, which has been neglected in the main body of the paper so far. In the following, the generation of synthetic spectra including the Ring effect is described (Sect. B1). Retrieval wavelength maps are shown and discussed in Sects. B2 and B3, which have been constructed for both measurement scenarios with retrievals applying I_0-corrected RCSs and a Ring spectrum.

B1 Generation of synthetic spectra and evaluation of spectra

The generation of synthetic spectra is performed analogous to the approach described in Sect. 3.1 and is the same for both measurement scenarios. First, a Fraunhofer reference spectrum $I_{K,0}$ and measurement spectrum I_K are constructed according to Eq. (1). The Ring effect is introduced into the generation of synthetic measurement by calculating a spectrum consisting only of the rotational Raman scattered (RRS) photons from the synthetic measurement spectrum I_K. The RRS spectrum $I_{K,RRS}$ is calculated using the software DOASIS, which assumes that N_2 and O_2 are the only molecules responsible for the RRS at a ratio 80 % to 20 %, respectively (Bussemer, 1993). It is assumed that 2 % of the total amount of photons present in the synthetic measurement spectrum I_K are inelastically scattered. The resulting optical density of the RRS spectrum represents a common value (e.g. Kattawar et al., 1981). I_K and $I_{K,RRS}$ are normalised to 98 % and 2 % of the integrated intensity of I_K, before being added to a new synthetic measurement $I_{K,R}$ including the Ring effect. As in Sect. 3.1, the high-resolution measurement spectrum $I_{K,R}$ is convolved with the instrumental slit function W to yield a synthetic spectrum $I_{M,R}$ at the resolution of the simulated instrument.

$$N = \int I_K(\lambda)\,d\lambda \tag{B1}$$

$$N_{RRS} = \int I_{K,RRS}(\lambda)\,d\lambda \tag{B2}$$

$$I_{K,R} = 0.98 \cdot I_K + 0.02 \cdot N/N_{RRS} \cdot I_{K,RRS} \tag{B3}$$

$$I_{M,R} = W * I_{K,R} \tag{B4}$$

It is important to note that this approach is simplified and that all RRS events are assumed to occur solely after the absorption processes. Consequently, the absorption structures of the trace gas are slightly reduced due to the filling in of absorption lines. Also, the results may not be directly transferred to measurements, because RRS events would occur continuously along the light path, before and after the absorption processes simulated here.

In typical DOAS retrievals, the Ring spectrum is calculated based on either the measured reference spectrum or a high-resolution solar reference spectrum (Table 1). Since I_0 in both measurement scenarios is the Fraunhofer solar reference spectrum at instrument resolution, a Ring spectrum was calculated from I_0 and appended to the set of the I_0-corrected RCSs. For both measurement scenarios, retrieval

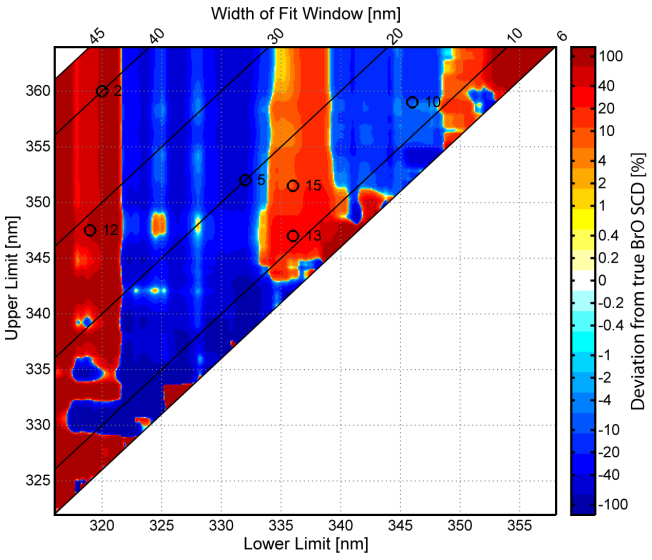

Fig. B1. Shown are deviations from the true SCD of BrO for the measurement scenario zenith DOAS, including the Ring effect and I_0-corrected RCSs in the retrieval. Compared to retrieval results without considering the Ring effect (Fig. 1), a general underestimation of the BrO SCDs can be observed. The areas of greater deviations remain similar with a strong dependency on the lower wavelength limit, with changes in sign at approximately 322 nm, 333 nm, 339 nm and 348 nm. However, the overestimation of BrO SCDs in Fig. 1 for lower wavelength limits $\approx$ 322–330 nm changed to an underestimation if the Ring effect is included.

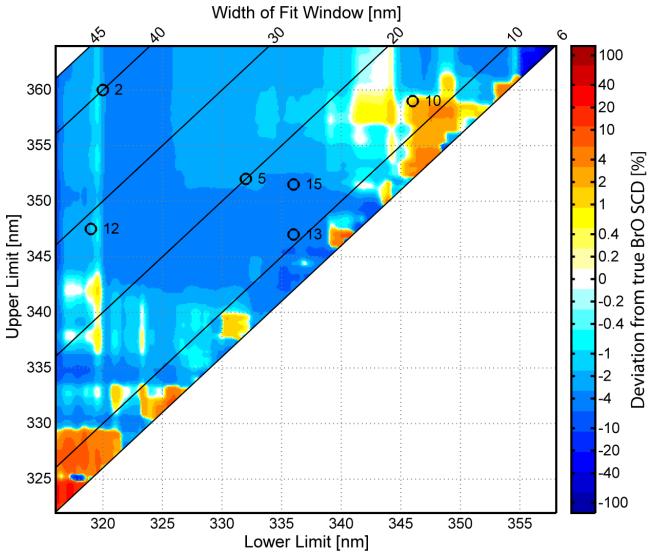

Fig. B2. The retrieval wavelength map for the measurement scenario of volcanic plumes including the Ring effect shows a general, expected underestimation of the true BrO SCD (compare Sect. B1 and Fig. 7, where the Ring effect is neglected for the measurement scenario of volcanic of plumes). Retrieval wavelength ranges, which may be relatively unaffected by the Ring effect, are indicated by the lack of variations in retrieved BrO SCDs at lower wavelength limits 320–337.5 nm and upper wavelength limit $>$ 342 nm.

wavelength maps were constructed for sets of I_0-corrected RCSs and a Ring spectrum in the evaluations.

B2 Results

B2.1 Zenith-sky DOAS

Figure B1 displays the result for zenith-sky DOAS. The general structure of the fitted BrO SCDs with varying retrieval wavelength interval is similar to Test I (Fig. 1). The strong dependency on the lower wavelength limit confirms the previous observations. Compared to Test I without considering the Ring effect in the main body of the paper, the following differences can be noted:

- BrO SCDs for lower wavelength limits $\approx$ 322–330 nm are underestimated, which were previously overestimated.
- BrO SCDs retrieved above a lower wavelength limit of $\approx$ 348 nm are now overestimated.
- BrO SCDs close to the true value are not retrieved at wavelength ranges with a lower limit $>$ 345 nm, which was the case in the previous Test I neglecting the Ring effect. Even at the retrieval interval of 346–359 nm (#10 Aliwell et al., 2002), the BrO SCD is underestimated by $\approx$ 8 %.
- The retrieval yields underestimated SCDs in general below a lower limit of $\approx$ 348 nm compared to Test I with I_0-corrected RCSs.

The left column of Fig. B3 depicts fit examples of the zenith-sky DOAS scenario at retrieval wavelength intervals #12, #5 and #10 (top to bottom). The best result is still obtained at the interval incorporating the longest wavelengths (#10), but the retrieved BrO SCD of 1.38×10^{14} molec cm^{-2} corresponds to an underestimation of $\approx$ 8 %. The observed residual structure is somewhat similar to the one observed in zenith-sky DOAS measurements (Aliwell et al., 2002, Fig. 5b).

B2.2 BrO in volcanic plumes

For the measurement scenario BrO in volcanic plumes, systematic deviations from the true BrO SCD (Fig. B2) are apparent with the majority of the deviations being below 5 %. In comparison to Test I and the zenith-sky DOAS scenario, the following observations are made:

- A strong dependency on the lower wavelength limit is not visible due to the missing strong O_3 absorptions and the narrow-band features of the Ring effect present over the whole spectral range.

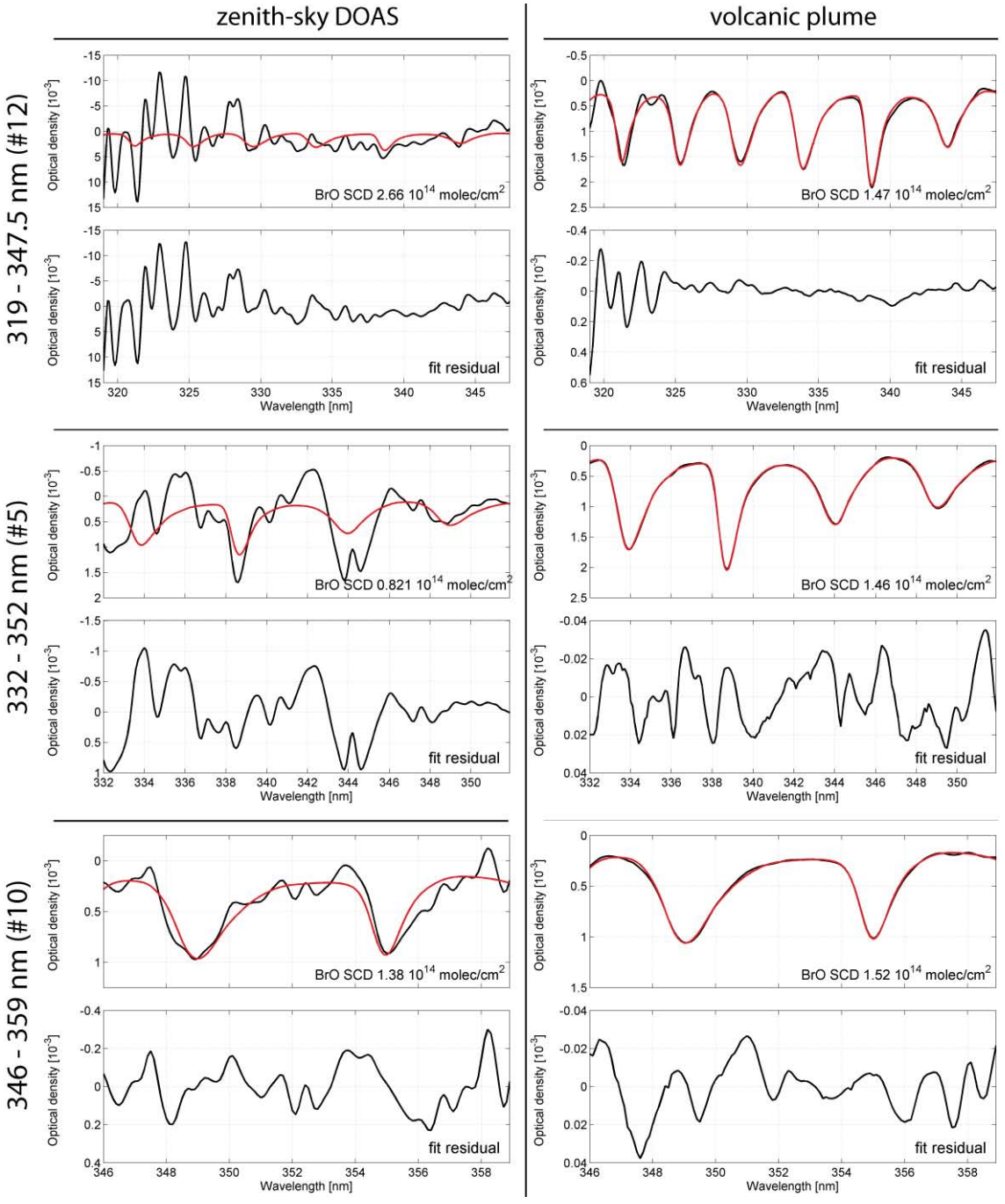

Fig. B3. Fit examples for selected wavelength intervals (#12, #5, #10 in Table 1) for the measurement scenarios zenith-sky DOAS (left column) and BrO in volcanic plumes (right column) including the Ring effect and I_0-corrected sets of RCSs. Compared to the fit examples of Test I (Figs. 4 and 9) with I_0-corrected RCSs, an increase in residual structures and deviation from the true BrO SCD are observed.

– Retrievals which are relatively independent on the chosen wavelength ranges are indicated by the lack of variations of BrO SCDs at lower wavelength limits 320–337.5 nm and upper wavelength limit > 342 nm.

– A negative offset of the retrieved BrO column densities is present at most intervals, also in comparison the Test I. This negative offset reaches up to 5 % in the wavelength intervals given above.

Examples of the fit are given in the right column of Fig. B3. Despite the negative offset of the retrieved BrO column densities, fits at the three depicted wavelength intervals do not exhibit strong residual features. Interval #12

(319–347.5 nm) shows the residual of highest peak to peak amplitude. It would not be unambiguously possible to judge solely from the residuals of the other retrievals, whether retrieval interval #5 (332–352 nm) or #10 (346–359 nm) yields a result closer to the true SCD.

B3 Discussion and conclusions

The results for both measurement scenarios are consistent with previous experience that the Ring effect is an important influence on retrievals of passive DOAS measurements. Even though the performed tests can not be unambiguously transferred to measurements because of the limitations of the Ring effect simulations, additional conclusions can be drawn.

First, the I_0 effect dominates in the scenario of zenith-sky DOAS measurements. The dependency on the lower wavelength limit already observed in Test I (Sect. 4.1.1), which can be attributed to the influence of insufficiently modelled O_3 absorption structures in the retrieval, shows that the I_0 effect is indeed the major source of error at lower wavelengths. At higher retrieval wavelengths, the errors introduced in the retrieval by the Ring effect prevent a successful retrieval of true BrO SCDs at wavelength ranges, which yielded correct results in Test I performed without the Ring effect.

Second, when the I_0 effect can be corrected sufficiently as in the measurement scenario of volcanic plumes, the malicious influence of the Ring effect on the retrieval becomes more prominent. Figure B2 shows that retrievals at all wavelengths are affected. Without the strong O_3 absorptions, the dependency on the lower retrieval wavelength limit is reduced in comparison to the other scenario. If the retrieval wavelength interval is sufficiently wide and includes strong BrO absorption lines, the results are not strongly affected by changes in retrieval wavelength intervals (lower wavelength limits 320–337.5 nm and upper wavelength limit $>$ 342 nm.)

Third, this region of wavelength intervals also clearly shows an effect present in both measurement scenarios: a negative offset of BrO SCDs is observed in comparison to retrievals neglecting the Ring effect (Test I) at most wavelengths. This may partly be caused by a filling in of absorption lines due to the calculated RRS after the trace gas absorptions are applied. However, the observed deviations from the true column are far greater than 2 % and other error sources must be responsible.

For instance, the Ring spectrum included in the fit is calculated from the Fraunhofer reference spectrum. If strong absorbers like O_3 are present as in the case of zenith-sky DOAS, an additional error is introduced because the filling in of absorption structures of trace gases is not considered. The treatment of the Ring effect as an additional absorber in the retrieval with its own absorption cross section is based on approximations (e.g. Platt and Stutz, 2008, and references therein), which may lead to the small residual structures observed. Possible cross correlations between different absorber cross sections and the Ring spectrum can be disregarded. Additional tests using a calculated Ring spectrum as additional absorber instead of a Raman spectrum showed that SCDs of trace gases were retrieved at negligible differences to columns retrieved in Test I neglecting the Ring effect.

Supplementary material related to this article is available online at: http://www.atmos-meas-tech.net/6/275/2013/amt-6-275-2013-supplement.zip.

Acknowledgements. L. Vogel and H. Sihler contributed equally to this work. The authors would like to thank both the atmospheric chemistry group in Heidelberg and the satellite remote sensing group in Mainz for thorough discussions during the development phase of the presented method, and also two anonymous referees for their valuable comments and suggestions. Funding for this work is gratefully acknowledged, and has been provided in part by the SOPRAN project (#03F0611F, by the BMBF, the German Federal Ministry of Education and Research), the Network for Observation of Volcanic and Atmospheric Change (NOVAC) by the European Commission Framework 6 Research Program and the International Max Planck Research School for Atmospheric Chemistry and Physics, Mainz (Germany).

Edited by: J. Stutz

References

Afe, O., Richter, A., Sierk, B., Wittrock, F., and Burrows, J.: BrO emission from volcanoes: A survey using GOME and SCIAMACHY measurements, Geophys. Res. Lett., 31, L24113, doi:10.1029/2004GL020994, 2004.

Aliwell, S., Roozendael, M. V., Johnston, P., Richter, A., Wagner, T., and Arlander, D.: Analysis for BrO in zenith-sky spectra: An intercomparison exercise for analysis improvement, J. Geophys. Res., 107, D14, doi:10.1029/2001JD000329, 2002.

Bani, P., Oppenheimer, C., Tsanev, V. I., Carn, S. A., Cronin, S. J., Crimp, R., Calkins, J. A., Charley, D., Lardy, M., and Roberts, T. R.: Surge in sulphur and halogen degassing from Ambrym volcano, Vanuatu, B. Volcanol., 71, 1159–1168, doi:10.1007/s00445-009-0293-7, 2009.

Begoin, M., Richter, A., Weber, M., Kaleschke, L., Tian-Kunze, X., Stohl, A., Theys, N., and Burrows, J. P.: Satellite observations of long range transport of a large BrO plume in the Arctic, Atmos. Chem Phys., 10, 6515–6526, doi:10.5194/acp-10-6515-2010, 2010.

Bobrowski, N. and Platt, U.: SO_2/BrO ratios studied in five volcanic plumes, J. Volcanol. Geoth. Res., 166, 147–160, 2007.

Boichu, M., Oppenheimer, C., Roberts, T. J., Tsanev, V., and Kyle, P. R.: On bromine, nitrogen oxides and ozone depletion in the tropospheric plume of Erebus volcano (Antarctica), Atmos. Environ., 45, 3856–3866, doi:10.1016/j.atmosenv.2011.03.027, 2011.

Burrows, J., Richter, A., Dehn, A., Deters, B., Himmelmann, S., and Orphal, J.: Atmospheric remote-sensing reference data from GOME - 2. Temperature-dependent absorption cross sections of O-3 in the 231–794 nm range, J. Quant. Spectrosc. Radiat. Transfer, 61, 509–517, doi:10.1016/S0022-4073(98)00037-5, 1999.

Bussemer, M.: Der Ring Effekt: Ursachen und Einfluß auf die Spektroskopischen Messungen Stratosphaerischer Spurenstoffe, Master's thesis, IUP, University Heidelberg, 1993.

Chance, K.: Analysis of BrO measurements from the Global Ozone Monitoring Experiment, Geophys. Res. Lett., 25, 3335–3338, doi:10.1029/98GL52359, 1998.

Chance, K.: OMI Algorithm Theoretical Basis Document – Volume IV, Tech. Rep., Smithsonian Astrophysical Observatory, Cambridge, MA, USA, 2002.

Chance, K., Kurosu, T., and Sioris, C.: Undersampling correction for array detector-based satellite spectrometers, Appl. Opt., 44, 1296–1304, doi:10.1364/AO.44.001296, 2005.

Coburn, S., Dix, B., Sinreich, R., and Volkamer, R.: The CU ground MAX-DOAS instrument: characterization of RMS noise limitations and first measurements near Pensacola, FL of BrO, IO, and CHOCHO, Atmos. Meas. Tech., 4, 2421–2439, doi:10.5194/amt-4-2421-2011, 2011.

Curci, G., Palmer, P. I., Kurosu, T. P., Chance, K., and Visconti, G.: Estimating European volatile organic compound emissions using satellite observations of formaldehyde from the Ozone Monitoring Instrument, Atmos. Chem. Phys., 10, 11501–11517, doi:10.5194/acp-10-11501-2010, 2010.

De Smedt, I., Van Roozendael, M., and Jacobs, T.: Optimization of DOAS settings for BrO fitting from SCIAMACHY nadir spectra – Comparison with GOME BrO retrievals, Tech. rep., Belg. Inst. for Space Aeron., Brussels, Belgium, available at: http://www.oma.be/BIRA-IASB/Molecules/BrO/BIRA_SCIABrO.pdf, 2004.

Doasis: DOAS Intelligent System Institute of Environmental Physics, University Heidelberg, Germany, available at: https://doasis.iup.uni-heidelberg.de/bugtracker/projects/doasis/, 2010.

Dorf, M.: Investigation of Inorganic Stratospheric Bromine using Balloon-Borne DOAS Measurements and Model Simulations, Ph.D. thesis, Combined Faculties for the Natural Sciences and for Mathematics, Ruperto Carola University of Heidelberg, Germany, 2005.

Fleischmann, O., Hartmann, M., Burrows, J., and Orphal, J.: New ultraviolet absorption cross-sections of BrO at atmospheric temperatures measured by time-windowing Fourier transform spectroscopy, J. Photochem. Photobiol. A, 168, 117–132, doi:10.1016/j.jphotochem.2004.03.026, 2004.

Grainger, J. F. and Ring, J.: Anomalous Fraunhofer line profiles, Nature, 193, 762 pp., doi:10.1038/193762a0, 1962.

Hebestreit, K., Stutz, J., Rosen, D., Matveiv, V., Peleg, M., Luria, M., and Platt, U.: DOAS measurements of tropospheric bromine oxide in mid-latitudes, Science, 283, 55–57, doi:10.1126/science.283.5398.55, 1999.

Heckel, A., Richter, A., Tarsu, T., Wittrock, F., Hak, C., Pundt, I., Junkermann, W., and Burrows, J. P.: MAX-DOAS measurements of formaldehyde in the Po-Valley, Atmos. Chem. Phys., 5, 909–918, doi:10.5194/acp-5-909-2005, 2005.

Hegels, E., Crutzen, P., Klupfel, T., Perner, D., and Burrows, J.: Global distribution of atmospheric bromine-monoxide from GOME on earth observing satellite ERS-2, GeoPhys. Res. Lett., 25, 3127–3130, doi:10.1029/98GL02417, 1998.

Hermans, C., Vandaele, A., and Fally, S.: Fourier transform measurements of SO_2 absorption cross sections: I. Temperature dependence in the 24 000–29 000 cm(-1) (345–420 nm) region, J. Quant Spectrosc. Radiat. Transfer, 110, 756–765, doi:10.1016/j.jqsrt.2009.01.031, 2009.

Heue, K.-P., Brenninkmeijer, C. A. M., Baker, A. K., Rauthe-Schöch, A., Walter, D., Wagner, T., Hörmann, C., Sihler, H., Dix, B., Frieß, U., Platt, U., Martinsson, B. G., van Velthoven, P. F. J., Zahn, A., and Ebinghaus, R.: SO_2 and BrO observation in the plume of the Eyjafjallajökull volcano 2010: CARIBIC and GOME-2 retrievals, Atmos. Chem. Phys., 11, 2973–2989, doi:10.5194/acp-11-2973-2011, 2011.

Hönninger, G., Leser, H., Sebastian, O., and Platt, U.: Ground-based measurements of halogen oxides at the Hudson Bay by active longpath DOAS and passive MAX-DOAS, Geophys. Res. Lett., 31, L04111, doi:10.1029/2003GL018982, 2004.

Huijnen, V., Eskes, H. J., Poupkou, A., Elbern, H., Boersma, K. F., Foret, G., Sofiev, M., Valdebenito, A., Flemming, J., Stein, O., Gross, A., Robertson, L., D'Isidoro, M., Kioutsioukis, I., Friese, E., Amstrup, B., Bergstrom, R., Strunk, A., Vira, J., Zyryanov, D., Maurizi, A., Melas, D., Peuch, V.-H., and Zerefos, C.: Comparison of OMI NO_2 tropospheric columns with an ensemble of global and European regional air quality models, Atmos. Chem. Phys., 10, 3273–3296, doi:10.5194/acp-10-3273-2010, 2010.

Jähne, B.: Digital Image Processing, Springer, 2005.

Kattawar, G. W., Young, A. T., and Humphreys, T. J.: Inelastic-Scattering in Planetary-Atmospheres. 1. The Ring Effect, without Aerosols, Astrophys. J., 243, 1049–1057, 1981.

Kern, C., Sihler, H., Vogel, L., Rivera, C., Herrera, M., and Platt, U.: Halogen oxide measurements at Masaya Volcano, Nicaragua using active long path differential optical absorption spectroscopy, B. Volcanol., 71, 659–670, doi:10.1007/s00445-008-0252-8, 2009.

Kern, C., Deutschmann, T., Vogel, L., Woehrbach, M., Wagner, T., and Platt, U.: Radiative transfer corrections for accurate spectroscopic measurements of volcanic gas emissions, B. Volcanol., 72, 233–247, doi:10.1007/s00445-009-0313-7, 2010.

Kraus, S. G.: DOASIS, A Framework Design for DOAS, Ph.D. thesis, University of Mannheim, available at: http://hci.iwr.uni-heidelberg.de/publications/dip/2006/Kraus_PhD2006.pdf, 2006.

Kurucz, R. L.: High resolution irradiance spectrum from 300 to 1000 nm, in: AFRL Transmission Meeting, AFRL Transmission Meeting, Lexington, Mass, available at: http://kurucz.harvard.edu/sun.html, 2005.

Lehmann, T.: Improving the sensitivity of spectroscopic measurements of atmospheric trace gases by modern signal processing algorithms, Ph.D. thesis, in preparation, IUP, University Heidelberg, 2013.

Leser, H., Honninger, G., and Platt, U.: MAX-DOAS measurements of BrO and NO_2 in the marine boundary layer, Geophys. Res. Lett., 30, 1537, doi:10.1029/2002GL015811, 2003.

Liao, J., Sihler, H., Huey, L. G., Neuman, J. A., Tanner, D. J., Friess, U., Platt, U., Flocke, F. M., Orlando, J. J., Shepson, P. B., Beine, H. J., Weinheimer, A. J., Sjostedt, S. J., Nowak, J. B., Knapp, D. J., Staebler, R. M., Zheng, W., Sander, R., Hall, S. R., and Ullmann, K.: A comparison of Arctic BrO measurements by chemical ionization mass spectrometry and long path-differential optical absorption spectroscopy, J. Geophys. Res.-Atmos., 116, D00R02, doi:10.1029/2010JD014788, 2011.

Mahajan, A. S., Plane, J. M. C., Oetjen, H., Mendes, L., Saunders, R. W., Saiz-Lopez, A., Jones, C. E., Carpenter, L. J., and McFiggans, G. B.: Measurement and modelling of tropospheric reactive

halogen species over the tropical Atlantic Ocean, Atmos. Chem. Phys., 10, 4611–4624, doi:10.5194/acp-10-4611-2010, 2010.

Marquard, L., Wagner, T., and Platt, U.: Improved air mass factor concepts for scattered radiation differential optical absorption spectroscopy of atmospheric species, J. Geophys. Res.-Atmos., 105, 1315–1327, doi:10.1029/1999JD900340, 2000.

Matveev, V., Peleg, M., Rosen, D., Tov-Alper, D., Hebestreit, K., Stutz, J., Platt, U., Blake, D., and Luria, M.: Bromine oxide – ozone interaction over the Dead Sea, J. Geophys. Res.-Atmos., 106, 10375–10387, doi:10.1029/2000JD900611, 2001.

Meller, R. and Moortgat, G.: Temperature dependence of the absorption cross sections of formaldehyde between 223 and 323 K in the wavelength range 225–375 nm, J. Geophys. Res.-Atmos., 105, 7089–7101, 2000.

Merten, A., Tschritter, J., and Platt, U.: Design of differential optical absorption spectroscopy long-path telescopes based on fiber optics, Appl. Opt., 50, 738–754, 2011.

Otten, C., Ferlemann, F., Platt, U., Wagner, T., and Pfeilsticker, K.: Groundbased DOAS UV/visible measurements at Kiruna (Sweden) during the SESAME winters 1993/94 and 1994/95., J. Atmos. Chem., 30, 141–162, doi:10.1023/A:1005810732347, 1998.

Platt, U. and Stutz, J.: Differential Optical Absorption Spectroscopy: Principles and Application, edited by: Guzzi, R., Lanzerotti, L., Imboden, D., and Platt, U., Springer Verlag, Berlin Heidelberg, Germany, 598 pp., doi:10.1007/978-3-540-75776-4, 2008.

Platt, U., Marquard, L., Wagner, T., and Perner, D.: Corrections for zenith scattered light DOAS, Geophys. Res. Lett., 24, 1759–1762, doi:10.1029/97GL01693, 1997.

Platt, U., Meinen, J., Pöhler, D., and Leisner, T.: Broadband Cavity Enhanced Differential Optical Absorption Spectroscopy (CE-DOAS) – applicability and corrections, Atmos. Meas. Tech., 2, 713–723, doi:10.5194/amt-2-713-2009, 2009.

Poehler, D., Vogel, L., Friess, U., and Platt, U.: Observation of halogen species in the Amundsen Gulf, Arctic, by active long-path differential optical absorption spectroscopy, Proc. Natl. Acad. Sci. USA, 107, 6582–6587, doi:10.1073/pnas.0912231107, 2010.

Prados-Roman, C., Butz, A., Deutschmann, T., Dorf, M., Kritten, L., Minikin, A., Platt, U., Schlager, H., Sihler, H., Theys, N., Van Roozendael, M., Wagner, T., and Pfeilsticker, K.: Airborne DOAS limb measurements of tropospheric trace gas profiles: case studies on the profile retrieval of O(4) and BrO, Atmos. Meas. Tech., 4, 1241–1260, doi:10.5194/amt-4-1241-2011, 2011.

Puķite, J., Kühl, S., Deutschmann, T., Platt, U., and Wagner, T.: Extending differential optical absorption spectroscopy for limb measurements in the UV, Atmos. Meas. Tech., 3, 631–653, doi:10.5194/amt-3-631-2010, 2010.

Richter, A., Wittrock, F., Eisinger, M., and Burrows, J.: GOME observations of tropospheric BrO in northern hemispheric spring and summer 1997, Geophys. Res. Lett., 25, 2683–2686, doi:10.1029/98GL52016, 1998.

Richter, A., Eisinger, M., Ladstätter-Weißenmayer, A., and Burrows, J.: DOAS Zenith Sky Observations: 2. Seasonal Variation of BrO over Bremen (53° N) 1994-1995, J. Atmos. Chem., 32, 83–99, doi:10.1023/A:1006077725894, 1999.

Richter, A., Wittrock, F., Ladstätter-Weißenmayer, A., and Burrows, J. P.: GOME measurements of stratospheric and tropospheric BrO, Adv. Space Res., 29, 1667–1672, doi:10.1016/S0273-1177(02)00123-0, 2002.

Roscoe, H. K., Fish, D. J., and Jones, R. L.: Interpolation errors in UV-visible spectroscopy for stratospheric sensing: Implications for sensitivity, spectral resolution, and spectral range, Appl. Opt., 35, 427–432, doi:10.1364/AO.35.000427, 1996.

Roscoe, H. K., Van Roozendael, M., Fayt, C., du Piesanie, A., Abuhassan, N., Adams, C., Akrami, M., Cede, A., Chong, J., Clémer, K., Friess, U., Gil Ojeda, M., Goutail, F., Graves, R., Griesfeller, A., Grossmann, K., Hemerijckx, G., Hendrick, F., Herman, J., Hermans, C., Irie, H., Johnston, P. V., Kanaya, Y., Kreher, K., Leigh, R., Merlaud, A., Mount, G. H., Navarro, M., Oetjen, H., Pazmino, A., Perez-Camacho, M., Peters, E., Pinardi, G., Puentedura, O., Richter, A., Schönhardt, A., Shaiganfar, R., Spinei, E., Strong, K., Takashima, H., Vlemmix, T., Vrekoussis, M., Wagner, T., Wittrock, F., Yela, M., Yilmaz, S., Boersma, F., Hains, J., Kroon, M., Piters, A., and Kim, Y. J.: Intercomparison of slant column measurements of NO_2 and O_4 by MAX-DOAS and zenith-sky UV and visible spectrometers, Atmos. Meas. Tech., 3, 1629–1646, doi:10.5194/amt-3-1629-2010, 2010.

Saiz-Lopez, A., Plane, J., and Shillito, J.: Bromine oxide in the mid-latitude marine boundary layer, GeoPhys. Res. Lett., 31, L03111, doi:10.1029/2003GL018956, 2004.

Salawitch, R. J., Canty, T., Kurosu, T., Chance, K., Liang, Q., da Silva, A., Pawson, S., Nielsen, J. E., Rodriguez, J. M., Bhartia, P. K., Liu, X., Huey, L. G., Liao, J., Stickel, R. E., Tanner, D. J., Dibb, J. E., Simpson, W. R., Donohoue, D., Weinheimer, A., Flocke, F., Knapp, D., Montzka, D., Neuman, J. A., Nowak, J. B., Ryerson, T. B., Oltmans, S., Blake, D. R., Atlas, E. L., Kinnison, D. E., Tilmes, S., Pan, L. L., Hendrick, F., Van Roozendael, M., Kreher, K., Johnston, P. V., Gao, R. S., Johnson, B., Bui, T. P., Chen, G., Pierce, R. B., Crawford, J. H., and Jacob, D. J.: A new interpretation of total column BrO during Arctic spring, Geophys. Res. Lett., 37, L21805, doi:10.1029/2010GL043798, 2010.

Sihler, H., Platt, U., Beirle, S., Marbach, T., Kühl, S., Dörner, S., Verschaeve, J., Frieß, U., Pöhler, D., Vogel, L., Sander, R., and Wagner, T.: Tropospheric BrO column densities in the Arctic derived from satellite: retrieval and comparison to ground-based measurements, Atmos. Meas. Tech., 5, 2779–2807, doi:10.5194/amt-5-2779-2012, 2012.

Stutz, J. and Platt, U.: Numerical analysis and estimation of the statistical error of differential optical absorption spectroscopy measurements with least-squares methods, Appl. Opt., 35, 6041–6053, doi:10.1364/AO.35.006041, 1996.

Stutz, J., Thomas, J. L., Hurlock, S. C., Schneider, M., von Glasow, R., Piot, M., Gorham, K., Burkhart, J. F., Ziemba, L., Dibb, J. E., and Lefer, B. L.: Longpath DOAS observations of surface BrO at Summit, Greenland, Atmos. Chem. Phys., 11, 9899–9910, doi:10.5194/acp-11-9899-2011, 2011.

Theys, N., Van Roozendael, M., Hendrick, F., Fayt, C., Hermans, C., Baray, J.-L., Goutail, F., Pommereau, J.-P., and De Mazière, M.: Retrieval of stratospheric and tropospheric BrO columns from multi-axis DOAS measurements at Reunion Island (21° S, 56° E), Atmos. Chem. Phys., 7, 4733–4749, doi:10.5194/acp-7-4733-2007, 2007.

Theys, N., Roozendael, M. V., Dils, B., Hendrick, F., Hao, N., and Maziere, M. D.: First satellite detection of volcanic bromine monoxide emission after the Kasatochi eruption, Geophys. Res. Lett., 36, L03809, doi:10.1029/2008GL036552, 2009.

Tuckermann, M., Ackermann, R., Golz, C., LorenzenSchmidt, H., Senne, T., Stutz, J., Trost, B., Unold, W., and Platt, U.: DOAS-observation of halogen radical-catalysed arctic boundary layer ozone destruction during the ARCTOC-campaigns 1995 and 1996 in Ny-Alesund, Spitsbergen, European-Geophysical-Society Symposium on Arctic Tropospheric Chemistry, The Hague, Netherlands, 6–10 May 1996, Tellus Series B, 49, 533–555, doi:10.1034/j.1600-0889.49.issue5.9.x, 1997.

Valks, P., Loyola, D., Hao, N., and Rix, M.: Algorithm Theoretical Basis Document for GOME-2 Total Column Products of Ozone, Minor Trace Gases, and Cloud Properties, Tech. Rep., Deutsches Zentrum für Luft und Raumfahrt, Oberpfaffenhofen, Germany, 2009.

Vandaele, A., Hermans, C., Simon, P., Carleer, M., Colin, R., and Fally, S.: Measurements of the NO_2 absorption cross-section from 42 000 cm(-1) to 10 000 cm(-1) (238–1000 nm) at 220 K and 294 K, J. Quant Spectrosc. Radiat. Transfer, 59, 171–184, doi:10.1016/S0022-4073(97)00168-4, 1998.

Vandaele, A., Hermans, C., and Fally, S.: Fourier transform measurements of SO_2 absorption cross sections: II. Temperature dependence in the 29 000-44 000 cm(-1) (227-345 nm) region, J. Quant Spectrosc. Radiat. Transfer, 110, 2115–2126, doi:10.1016/j.jqsrt.2009.05.006, 2009.

Vogel, L.: Volcanic plumes: Evaluation of spectroscopic measuremetns, early detection and bromine chemistry, Ph.D. thesis, Combined Faculties for the Natural Sciences and for Mathematics, Ruperto Carola University of Heidelberg, Germany, available at: http://www.ub.uni-heidelberg.de/archiv/13219, 2011.

von Glasow, R.: Atmospheric chem in volcanic plumes, Proc. Natl. Acad. Sci. USA, 107, 6594–6599, doi:10.1073/pnas.0913164107, 2010.

Wagner, T. and Platt, U.: Satellite mapping of enhanced BrO concentrations in the troposphere, Nature, 395, 486–490, doi:10.1038/26723, 1998.

Wagner, T., Chance, K., Frieß, U., Gil, M., Goutail, F., Hönninger, G., Johnston, P., Karlsen-Tørnkvist, K., Kostadinov, I., Leser, H., Petritoli, A., Richter, A., Van Roozendael, M., and Platt, U.: Correction of the ring effect and I0effect for DOAS observations of scattered sunlight, ESA Technical Report, 2002.

Wagner, T., Ibrahim, O., Sinreich, R., Frieß, U., von Glasow, R., and Platt, U.: Enhanced tropospheric BrO over Antarctic sea ice in mid winter observed by MAX-DOAS on board the research vessel Polarstern, Atmos. Chem. Phys., 7, 3129–3142, doi:10.5194/acp-7-3129-2007, 2007.

Wagner, T., Beirle, S., and Deutschmann, T.: Three-dimensional simulation of the Ring effect in observations of scattered sun light using Monte Carlo radiative transfer models, Atmos. Meas. Tech., 2, 113–124, doi:10.5194/amt-2-113-2009, 2009.

Wahner, A., Ravishankara, A. R., Sander, S. P., and Friedl, R. R.: Absorption cross-section of BrO between 312 and 385nm at 298 and 223K, Chem. Phys. Lett., 152, 507–512, 1988.

Wenig, M., Jähne, B., and Platt, U.: Operator representation as a new differential optical absorption spectroscopy formalism, Appl. Opt., 44, 3246–3253, 2005.

Wilmouth, D. M., Hanisco, T. F., Donahue, N. M., and Anderson, J. G.: Fourier transform ultraviolet spectroscopy of the A (2)Pi(3/2) ¡- X (II3/2)-I-2 transition of BrO RID A-2329-2008, J. Phys. Chem. A, 103, 8935–8945, doi:10.1021/jp991651o, 1999.